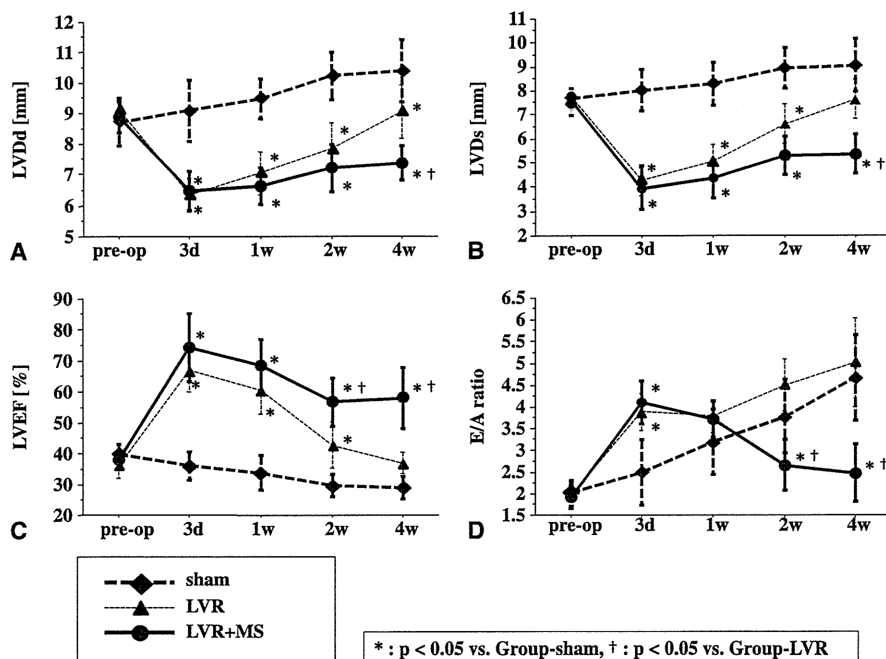

FIGURE 1. Serial echocardiographic study revealed significant decrease in left ventricular chamber size and significant increase in left ventricular ejection fraction by left ventricular restoration (LVR) in group LVR and in group LVR+ myoblast sheets (MS). However, gradual redilatation of left ventricular chamber and decrease of ejection fraction was observed in group LVR. Those later deteriorations were prevented in group LVR+MS, and the differences in chamber size and ejection fraction were significant between group LVR and group LVR+ MS 4 weeks after the operation. Changes in echocardiographic parameters before and after the operation. (A) Left ventricular dimension at end-diastole (LVDd), (B) left ventricular dimension at end-systole (LVDs), (C) Left ventricular ejection fraction (LVEF), (D) mitral valve E/A ratio. *P0.05 vs. group sham; †P0.05 vs. group LVR.

However, impairment of diastolic function and late remodeling are great concerns after LVR for ischemic cardiomyopathy (*5–7*), and the long-term effect of LVR is still controversial. Although LVR that is performed together with coronary artery bypass grafting (CABG) has been suggested to reduce the rate of hospitalization and improve ventricular function to a greater degree than CABG alone on the basis of a small, nonrandomized, case-control study (*8*), recently conducted multicenter, nonblinded, randomized trial (the Surgical Treatment for Ischemic Heart Failure [STICH] trial) have revealed that LVR does not improve the symptoms, exercise tolerance, rate of death, or hospitalization in patients with ischemic heart disease and severe LV dysfunction compared with CABG alone (*5*).

On the other hand, cell transplantation into impaired myocardium, also known as cellular cardiomyoplasty, has been investigated (*9*, *10*). Recently, we have developed a new cell delivery method by the means of cell sheet, in which autologous skeletal myoblasts were transplanted in sheet form, and reported that this method was effective especially in the attenuation of LV dilatation and the improvement of LV diastolic function (*11–14*). On the basis of these findings, we hypothesized that skeletal myoblast sheet (MS) implantation may attenuate the disadvantageous effects and enhance the advantageous effects of LVR. Using a rat model of chronic myocardial infarction model, we investigated whether MS implantation combined with LVR can attenuate the redilatation and diastolic dysfunction of LV after LVR.

RESULTS

Changes in Cardiac Function by LVR and LVR Combined With MS

Two weeks after left anterior descending coronary artery (LAD) ligation, severe dilatation of the LV chamber and severe asynergy of the anterior wall were observed in all the rats. By excluding the large akinetic or dyskinetic area of the LV anterior wall, LV dimension at end-diastole (LVDd) and end-systole (LVDs) significantly decreased and left ventricular ejection fraction (LVEF) significantly increased in group LVR and in group LVR+MS 3 days after treatment (Fig. 1). However, gradual LV redilatation and decrease of LVEF were observed in group LVR. MS implantation combined with LVR attenuated those later deteriorations of LV function significantly in group LVR+MS (Fig. 1). Mitral valve *E*/*A* ratio showed significant restrictive pattern after LVR. In group LVR, the restrictive pattern progressed even further with time. However, addition of the MS implantation attenuated the progression of the restrictive pattern (Fig. 1).

Hemodynamic Improvement by LVR Combined With MS

Table 1 shows the results of the hemodynamic study by cardiac catheterization 4 weeks after the second operation. The basic hemodynamic indices revealed that LV end-diastolic pressure (EDP) and the time constant of isovolumic relaxation (τ) were significantly lower in group LVR+MS than in group LVR or group sham. Load-independent parameters measured by pressure-volume loop analysis revealed that end-systolic pressure (ESP) volume relationship was significantly higher in group LVR+MS than in the other two groups. EDP volume relationship (EDPVR) was significantly lower in group LVR+MS than in the other two groups.

Histological Impact of the MS on the Failing Heart

Figure 2 shows the typical cross section of the whole hearts 4 weeks after the operation from each group. Severe dilatation of the LV chamber and thinning of the LV wall were observed in group sham (Fig. 2A). In group LVR, although infracted area was excluded and smaller than that in group sham, LV chamber was markedly dilated (Fig. 2B). Also severe dilatation of the right ventricular chamber was observed. In group LVR+MS, the size of the LV chamber and the thickness of the LV wall were well preserved compared

Copyright © 2012 Lippincott Williams & Wilkins. Unauthorized reproduction of this article is prohibited.

TABLE 1. Hemodynamic indices 4 weeks after the operation

Group	Sham	LVR	LVR+MS
Basic hemodynamic indices			
HR (bpm)	219 ± 37	206 ± 20	231 ± 32
ESP (mm Hg)	60.9 ± 7.7	63.0 ± 13.9	73.0 ± 11.3[a]
EDP (mm Hg)	5.1 ± 2.2	9.0 ± 6.6	2.0 ± 1.0[a,b]
τ (msec)	21.3 ± 2.4	19.8 ± 2.2	14.4 ± 1.2[a,b]
Load independent parameters analyzed by pressure-volume loop			
ESPVR (mm Hg/ml)	1896 ± 906	1364 ± 661	4722 ± 2416[a,b]
EDPVR (/ml)	50 ± 36	42 ± 23	13 ± 6[a,b]
PRSW (mm Hg)	37.1 ± 24.3	33.0 ± 24.2	45.2 ± 32.7

[a] $P < 0.05$ vs. group sham.
[b] $P < 0.05$ vs. Group-LVR.
HR, heart rate; ESP, end-systolic pressure; EDP, end-diastolic pressure; τ, time constant of isovolumic relaxation; ESPVR, end-systolic pressure-volume relationship; EDPVR, end-diastolic pressure-volume relationship; PRSW, preload-recruitable stroke work.

with the other groups (Fig. 2C). The LV wall thickness was significantly larger in group LVR+MS than in the other two groups (vs. group sham and group LVR, P<0.05) (Fig. 3A). The degree of cardiac fibrosis was significantly smaller in group LVR+MS than in the other two groups (vs. group sham and group LVR, P<0.05) (Figs. 3B and 4A–C). Myocyte size was also significantly smaller in group LVR+MS than in the other two groups (vs. group sham and group LVR, P<0.05) (Figs. 3C and 4D–F). Vascular density of the LV lateral wall, the area where MS were applied in group LVR+MS, was significantly higher in group LVR+MS than in the other two groups (vs. group sham and group LVR, P<0.05) (Figs. 3D and 4G–I).

Suppression of Probrotic Agent Gene Expression by MS

Reverse transcription polymerase chain reaction analysis 4 weeks after the second operation revealed significantly suppressed expression of the profibrotic gene transforming growth factor-beta (TGF-β), Smad2, and reversion-inducing cysteine-rich protein with Kazal motifs (RECK) in group LVR+MS than in the other two groups (vs. group sham and group LVR, P<0.05) (Fig. 5A–C).

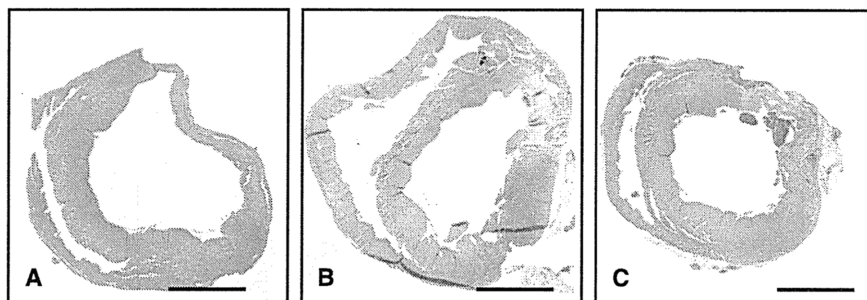

FIGURE 2. Cross section of the whole hearts 4 weeks after the operation from each group (hematoxylin-eosin staining). (A) group sham, (B) group LVR, (C) group LVR + MS.

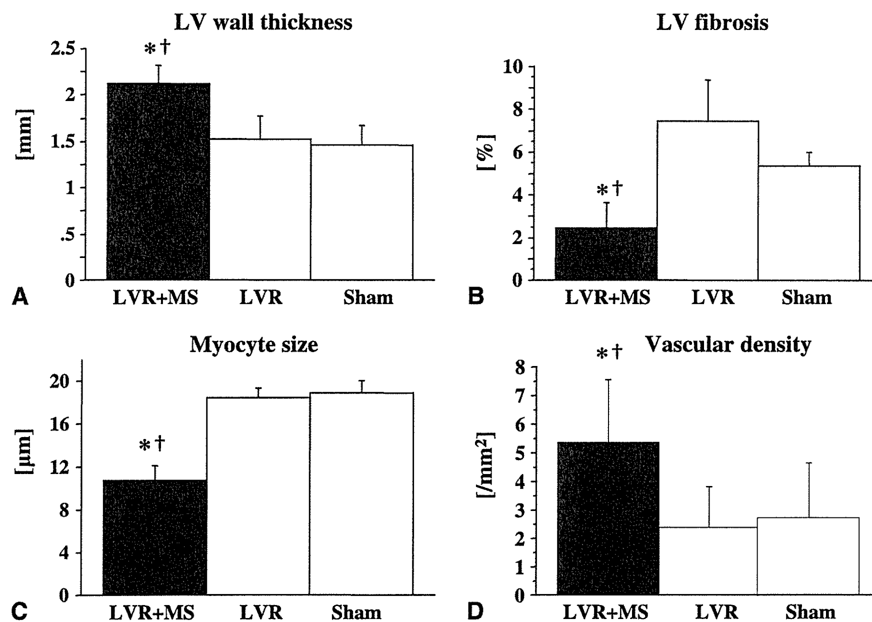

FIGURE 3. The left ventricular (LV) wall thickness was significantly larger in group left ventricular restoration (LVR)+myoblast sheets (MS) than in the other two groups 4 weeks after the operation (A). The degree of cardiac fibrosis (B) and myocyte size (C) were also significantly smaller in group LVR+MS than in the other two groups. The vascular density in the LV lateral wall, where MS were applied in group LVR+MS, were significantly higher in group LVR+MS than in the other two groups (D).

Copyright © 2012 Lippincott Williams & Wilkins. Unauthorized reproduction of this article is prohibited.

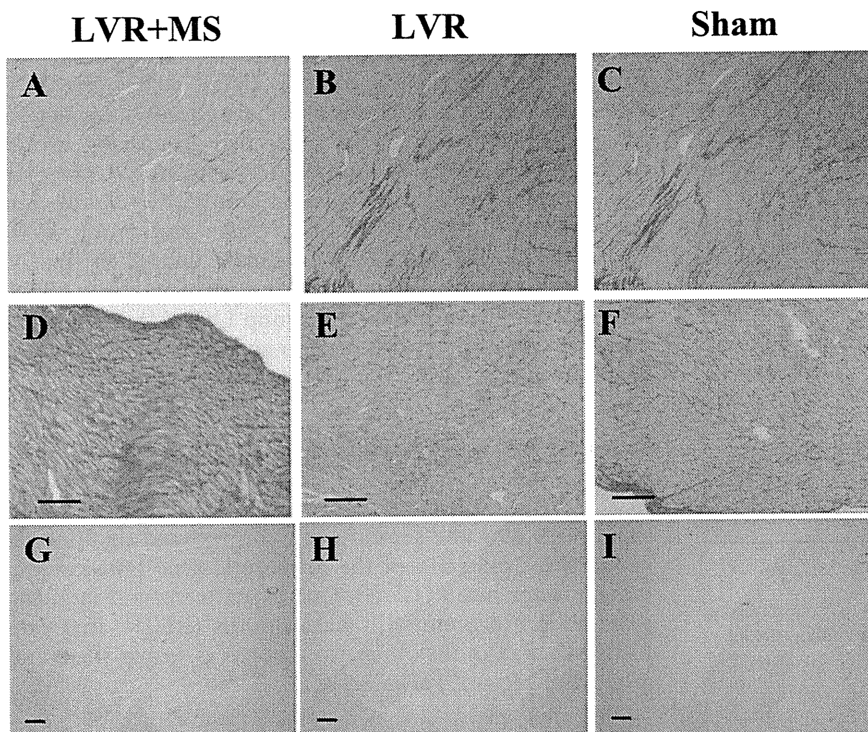

FIGURE 4. Picrosirius-red staining of myocardium from noninfarcted regions (A, B, C) and periodic acid-Schiff-stained myocardium from noninfarcted regions (D, E, F, bar=200 μm). Picrosirius-red staining of myocardium from noninfarcted regions. Sections of myocardium stained with antibody to von Willebrand factor (G, H, I, bar=300 μm).

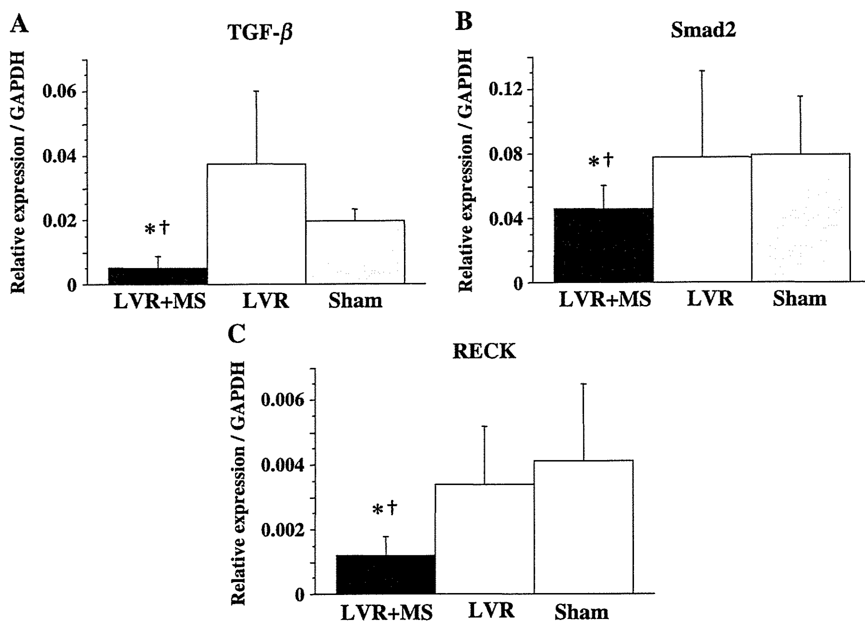

FIGURE 5. Reverse transcription polymerase chain reaction (RT-PCR) analysis 4 weeks after the second operation revealed significantly suppressed expression of the profibrotic gene transforming growth factor-beta (TGF-β) (A), Smad2 (B), and RECK (C) in group left ventricular restoration (LVR)+myoblast sheets (MS) than in the other two groups.

Engrafted Cell Survival

To evaluate the survival of engrafted cell on the recipient LV, MS made from male rats were implanted on the female LV, and surviving cell numbers were examined by detecting the Y chromosome-specific and gender consensus genes. To confirm the accuracy of the measurements, MS made from known numbers of male myoblasts were implanted on the LV wall of a female rat ex vivo, and a standard curve was prepared to determine the ratio of male cells to female cells and the relationship to the number of male cells. The correlation coefficient for the standard curve was 0.9716, indicating a significant correlation. The number of surviving engrafted cells was calculated using this standard curve (*15*). The number of cells detected on the day of implantation was approximately 64% of the engrafted cells (five layers of MS, with 3.0×10^6 myoblasts in each sheet). Surviving cells decreased to 69% of those in day 0. Although the number continued to decrease with time, 13% of those cells were still surviving on the LV wall 4 weeks after MS implantation (Fig. 6A).

Immunostaining of the green fluorescent protein (GFP) revealed that myoblasts sheets made from GFP transgenic rats

Copyright © 2012 Lippincott Williams & Wilkins. Unauthorized reproduction of this article is prohibited.

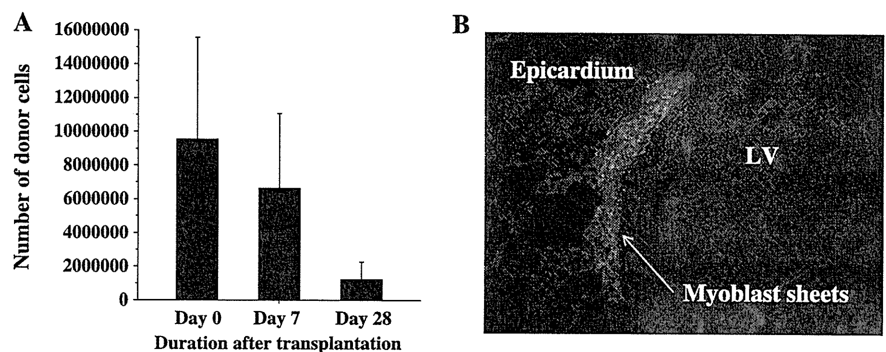

FIGURE 6. Survival of donor cells in recipient hearts. (A) Number of surviving engrafted cells in recipient hearts. Although the number of donor cells decreased with time, the surviving engrafted cells were still detectable 28 days after transplantation. (B) Immunostaining of the green fluorescent protein. Transplanted myoblast sheets were still detectable 28 days after the surgery.

were still detectable on the epicardium of LV wall 28 days after implantation (Fig. 6B).

DISCUSSION

Impairment of diastolic function and late remodeling are concerns after LVR for ischemic cardiomyopathy (*5–7*). Dor et al. (*6*) have reported the late redilatation of LV after LVR in their clinical experiences, and Nishina et al. (*16*) have developed a rat model that reproduces this clinical situation, in which model an infracted area of the LV anterior wall was simply plicated. Although LV configuration and function improved after the operation, LV chamber gradually redilated and LV function decreased, and the initial improvement almost disappeared in 4 weeks.

Using this same model, we implanted the skeletal MS concomitantly with LVR to investigate the ability of MS to overcome the drawbacks of the LVR. In this study, MS implantation attenuated the LV redilatation and decrease in EF after LVR. It was also shown by echocardiographic study and pressure-volume loop analysis that MS attenuated the impairment of diastolic function after LVR. Histological examination revealed that MS induced the angiogenesis in the myocardium where they were applied, and decreased the degree of myocardial fibrosis. MS controlled the gene expression that may regulate the myocardial fibrosis (TGF-β, Smad2, and RECK), and suppressed myocardial fibrosis. The number of viable myoblasts implanted on the LV wall concomitantly with LVR decreased with time, but they were still detectable on the LV wall 28 days after implantation. The surviving cells detected on the LV wall 28 days after transplantation were only 13% of those detected on the day of transplantation. However, to enhance the survivability and effectiveness of implanted cells, we have developed new additional therapy such as transfection of the gene for hepatocyte growth factor (HGF) (*17*) or omentum flap (*18*) combined with cell transplantation, and reported the efficacies of these additional therapies in the previous studies.

The mechanism of recovery of cardiac function by autologous MS are considered as combination of restoration of the LV wall by the MS, that is "girdling effect," and biological effects of the cytokines such as stromal-derived factor 1 (SDF-1), HGF, and vascular endothelial growth factor (VEGF) paracrined from sheet-shaped autologous myoblasts, that is "paracrine effect." SDF-1 is known to mobilize and recruit stem cells and leads to neovascularization (*19, 20*) and is secreted in skeletal muscle tissue (*21*). HGF is an angiogenic and antifibrotic factor (*22*), and VEGF is also a potent angiogenic factor (*23*). In the previous reports with animal models, we have demonstrated that the gene expressions of SDF-1, HGF, and VEGF were significantly higher in the hearts treated with MS than in hearts treated with myoblasts injection or with medium injection (*11, 14, 24*). As results of those enhanced gene expression, the hearts treated with MS showed higher number of hematopoietic stem cells in the treated area (*11*), greater vascularity (*11, 12, 14*), decreased cardiac fibrosis (*11–14, 24*), decreased apoptotic cells (*13*), and increased proliferative cells (*13*). Moreover, those effects were enhanced as the number of transplanted MS increased (*14*). Sekiya et al. (*14*) reported that the effect of the MS was maximally enhanced when it was implanted on the impaired myocardium in five layers, compared with three or one layer. Based on these data and experiences in our own laboratory, we chose the skeletal myoblasts as donor of cell sheets in this study, and decided the cell number and the layer number of the MS. In this study, we reconfirmed that angiogenesis was induced and fibrosis was suppressed by MS. It is considered that the angiogenesis enhanced the myocardial microcirculation and improved the myocardial ischemia, and resulted in attenuation of myocardial fibrosis and late remodeling. Instead of the well-known key factors secreted by MS such as SDF-1, HGF, and VEGF, we investigated the other signals that are known to control the degree of tissue fibrosis such as TGF-β, Smad, and RECK. TGF-β is a known profibrotic cytokine that has been demonstrated to induce cardiac fibrosis (*25*). The effect of TGF-β in the heart is primarily mediated though Smad2 phosphorylation (*26*). The TGF-β-Smad pathway seems to be involved in the activation of collagen-gene promoter sites, increasing DNA translation of collagen I. In this study, it was clearly proved that MS suppress the TGF-β-Smad pathway leading to the attenuation of cardiac fibrosis. RECK is known to be one of the inhibitors of metalloproteinases (*27*) and believed to be an important regulator of cardiac extracellular matrix. Although in this study we could not evaluate the matrix metalloproteinase (MMP) and tissue inhibitors of metalloproteinase activity, MS may activate the MMP acting through the suppression of RECK, leading to the reduction of fibrosis. It was shown for the first time that MS suppressed the degree of myocardial fibrosis by regulating those signals. The mechanisms by which MS regulate those signals remain to be investigated.

We also revealed that LV wall thickness was maintained and LV dilatation was attenuated by MS after LVR. From Laplace's law, this might have led to decrease in

Copyright © 2012 Lippincott Williams & Wilkins. Unauthorized reproduction of this article is prohibited.

LV wall stress and attenuation of the myocardial cellular hypertrophy.

In our previous study, we reported that MS increased elastin in the myocardium where the MS were implanted, and this might have contributed to the improvement in diastolic function (*14*). In this study, all the data acquired from echocardiography (mitral *E*/*A* ratio), catheter study (LVEDP, τ, and EDPVR), and histological study (fibrosis) revealed improvement of diastolic function by the MS.

One of the unique points of this study, compared with the previous studies with skeletal MS, was that the MS were applied to the viable area of the myocardium in this study. One of the most important mechanisms of the myocardial improvements by MS is considered paracrine effect of cytokines secreted from the skeletal myoblast. From this point of view, it is anticipated that the greater the number of the viable cells in the area of myocardium where the MS is attached, the greater the effect of the MS. This study is different from the previous studies in the point that the impaired myocardium was excluded by surgical LVR and the skeletal MS were attached to the remaining viable area of the myocardium. In the preliminary experiment of this study, we have also included the "MS only group" in the study groups. As reported in the previous studies, MS showed a certain effects and prevented the deterioration of the heart function compared with sham group. However, the comparisons between the group LVR+MS and "MS only group" were complicated because the conditions of the myocardium in which the MS were applied were different, so we excluded this group from the final design of this study.

Using the rat LVR model, other additional treatments such as administration of angiotensin-converting enzyme inhibitor (*28*), chymase inhibitor (*29*), or transplantation of fetal cardiomyocyte by needle injection (*30*) were reported to prevent the late remodeling after LVR in some extent. Not like the single medical treatments mentioned above, MS implantation affects on cardiac function by integrated pathway of angiogenesis, antifibrosis, mechanical unloading of the LV wall stress, and possibly other unknown mechanisms. MS implantation is supposed to be more effective than single medical treatment. As a cell delivery method, it is known that direct intramyocardial injection has several disadvantages, including cell loss caused by leakage of injected cells from the myocardium, poor survival of the grafted cells, myocardial damage after mechanical injury by the needle, and subsequent acute inflammation. MS implantation is a useful method to overcome these disadvantages, and we have reported the superiority of the myocardial sheets implantation to needle injection (*11–13*).

This study has some limitations. In this rat model, the area of myocardial infarction is not identical in all the rats 2 weeks after ligating the coronary artery, and thus the size of the LV and the degree of impairment of diastolic function are not identical in all the rats after LVR. Second, the surgery for excluding the infarction was carried out by imbrication stitches, and this is different from the actual procedure in the clinical setting, excision and re-sculpting of the left ventricle as described by Dor et al. (*6*). Additionally, we chose rats with large akinetic area as a myocardial infarction model and aggressively plicated this area to reproduce "the failing situation" after LVR. This situation may not be directly applied to clinical settings. However, we consider that the effectiveness of MS to attenuate impairment of diastolic function and late remodeling after LVR was shown by this model. We also recognize some limitations in our study with regard to the analysis of the mechanisms in which the MS reduce the cardiac fibrosis. Although we have demonstrated the enhanced gene expression of smad and RECK, further study is needed to analyze the level of gene expression of collagens, MMPs, and tissue inhibitors of metalloproteinases to show the activation of Smad2 and RECK protein.

In conclusion, skeletal MS implantation attenuated the impairment of diastolic function and the late remodeling after LVR in rat myocardial infarction model. It is suggested that MS implantation may improve the long-term outcome of LVR for ischemic heart disease.

MATERIALS AND METHODS

Animal Care

All experimental procedures and protocols used in this investigation were reviewed and approved by the institutional animal care and use committee and are in accordance with the National Institutes of Health Guide for the Care and Use of Laboratory Animals (NIH Publication No. 85-23, Revised 1996).

Isolation of Myoblasts and Construction of MS

Myoblasts were isolated from the skeletal muscle of the anterior tibialis from 3-week-old male Lewis rats and cultured as previously described (*11–14*). They were dissociated from the culture dishes with trypsin-ethylenediaminetetraacetic acid and reincubated on 35-mm temperature-responsive culture dishes (UpCell, Cellseed, Tokyo, Japan) at 37°C, with cell number adjusted to 3.0×10^6 per dish. More than 70% of these cells were actin-positive and 40% to 50% were desmin-positive (*14*). After 24 hr, the dishes were incubated at 20°C for 30 min. During that time, the MS detached spontaneously to generate free-floating, monolayer cell sheets. After detachment, the area of the sheets decreased to 1.00±0.05 cm^2, while the thickness increased to 100±10.0 μm (*14*). For the immunostaining of the engrafted MS, myoblasts were isolated from GFP transgenic Lewis rats and made into cell sheets in the same way as described earlier.

Myocardial Infarction Model

Eight-week-old male Lewis rats were used (220–250 g; Seac Yoshitomi Ltd. Fukuoka, Japan). The rats were anesthetized with ketamine (90 mg/kg) and Xylazine (10 mg/kg), and myocardial infarction was induced by ligation of LAD under mechanical ventilation. Two weeks after the ligation, baseline cardiac functions were measured by echocardiography, and rats that fulfill the following criteria were selected for further experiment: large akinetic or dyskinetic area in the anterior wall of the LV, LVDd 9.0±1.0 mm, and LVEF 35%±5%. For the quantitative study of the engrafted cell fate, 8-week-old female Lewis rats were used and myocardial infarction model was made in the same way as described earlier.

Experimental Groups

Male rats were randomized into three groups: 15 rats underwent only rethoracotomy (group sham), 15 underwent LVR (group LVR), and 15 underwent LVR, which was immediately followed by MS implantation (group LVR+MS). In group LVR and group LVR+MS, LVR was performed as follows: three to four mattress stitches with 7-0 polypropylene sutures were placed just onto the border line between infarcted and intact myocardium, and the infarcted myocardium was excluded (*16*). In group LVR+MS, five layers of MS were attached directly to the intact myocardium without sutures subsequently to LVR. After detachment from the temperature-responsive dish, each sheet was picked up individually and applied to the surface of the heart. After 3 to 5 min, subsequent sheets were applied and a total of five layers of MS were implanted. All the female rats underwent implantation of MS made from male rats concomitantly with LVR for the engrafted cell fate analysis. Additionally, three rats underwent implantation of the MS made from GFP positive

Copyright © 2012 Lippincott Williams & Wilkins. Unauthorized reproduction of this article is prohibited.

myoblasts after LVR in the same way as group LVR+MS for immunostaining of implanted MS.

Echocardiography

LV functions of all the treated rats were monitored by echocardiography at baseline (2 weeks after LAD ligation), 3 days, 1 week, 2 weeks, and 4 weeks after the second operation. Echocardiography was performed with a SONOS 5500 (Agilent Technologies, Palo Alto, CA) using a 12-MHz annular array transducer under anesthesia with inhalation of isoflurane. The hearts were imaged in short-axis 2D views at the level of the papillary muscles, and the LVDs and LVDd were determined. LVEF was calculated by Pombo's method, as EF (%)=$\{(LVDd^3-LVDs^3)/LVDd^3\}\times 100$. All the echocardiographic studies were performed by a single investigator who was blinded to the treatment groups and the results were agreed by all the other investigators.

Hemodynamic Study and Data Analysis

Four weeks after the second operation, after the last echocardiographic study, all the rats were ventilated again. Re-re-thoracotomy was performed and the LV apex was dissected carefully to minimize hemorrhaging. A silk thread was placed under the inferior vena cava just above the diaphragm to change the LV preload. After a purse string suture was attached to the LV apex with 7-0 polypropylene, the conductance catheter (Unique Medical Co., Tokyo, Japan) was inserted through the LV apex toward the aortic valve along the longitudinal axis of the LV cavity and then fixed. A Miller 1.4 Fr pressure-tip catheter (SPR-719, Millar Instruments, Houston, TX) was also inserted from the LV apex and fixed. The conductance system and the pressure transducer controller (Integral 3 [VPR-1002], Unique Medical Co.) were set as previously reported (*31*). The pressure-volume loops and intracardiac electrocardiogram were monitored online, and the conductance, pressure, and intracardiac electrocardiographic signals were analyzed with Integral version 3 software (Unique Medical Co.) (*31*). Under stable hemodynamic conditions, the baseline indices were initially measured and then the pressure-volume loop was drawn during the inferior vena cava occlusion and analyzed.

The following indices were calculated as the baseline LV function: heart rate, ESP, EDP, and τ. ESP volume relationship and EDPVR were determined by pressure-volume loop analysis as load-independent measures of the LV function. All the catheter studies were performed by a single investigator who was blinded to the treatment groups and the results were agreed by all the other investigators.

Histological Study

After all measurements were finished, the rats were killed for histological study. In eight rats from each group, LV myocardial specimens were obtained and fixed with 10% buffered formalin and embedded in paraffin. Hematoxylin-eosin staining was performed for the measurement of the ventricular wall thickness. The thickness of the ventricular wall was measured at two points from the LV posterior area and two points from the interventricular septum, and results were expressed as the average of the four points. Picrosirius red staining was performed to detect myocardial fibrosis. Myocardial fibrosis was expressed as percent fibrosis, the fraction of red-stained area in total myocardium, with results obtained from 10 fields per section per animal from LV lateral and posterior wall. Also periodic acid-Schiff staining was performed to examine the degree of cardiomyocyte hypertrophy. Myocyte size was determined by point-to-point perpendicular lines drawn across the cross-sectional area of the cell at the level of the nucleus. The results were expressed as the average diameter of 40 myocytes randomly selected from the LV lateral and posterior wall. To label vascular endothelial cells, so that blood vessels could be counted, immunohistochemical staining for factor VIII-related antigen was performed according to a modified protocol. We used EPOS-conjugated antibody to factor VIII-related antigen coupled with HRP (Dako EPOS Anti-Human von Willebrand Factor/HRP, Dako) as primary antibody. The stained vascular endothelial cells were counted under a light microscope. Results were expressed as the number of blood vessels/mm^2.

Measurement Probrotic Agent Gene Expression 4 Weeks After LVR and MS Implantation

In the remaining seven rats from each group, the myocardium from the LV lateral wall, the area where MS were applied in group LVR+MS, were also stored in RNAlater solution (QIAGEN, Hilden, Germany). Total RNA was extracted with the RNeasy mini kit (QIAGEN), and relative levels of RNA transcripts were measured by the real-time quantitative reverse transcription polymerase chain reaction technique using the ABI PRISM 7700 Sequence Detection System. The measurement of the mRNA expression of TGF-β, Smad2, and RECK was performed in triplicate. The results are expressed after normalization for glyceraldehydes-phosphate dehydrogenase.

Quantitative and Histological Evaluation of Engrafted Cell Survival

Intact hearts from female Lewis rats were collected, freed of the right ventricular free wall, and transplanted with MS made from known numbers (3.0×10^2, 3.0×10^3, 3.0×10^4, 3.0×10^5, 3.0×10^6, or 3.0×10^7, n=3 each) of male Lewis rats myoblast. Samples were homogenized and analyzed for the levels of *sry* and *il2*, which are Y chromosome-specific and gender consensus genes, respectively. An estimate of the fraction of donor cells was calculated as $2\times$ *sry*/*il2*$\times100$, and standard curves were constructed to determine the myoblast number from the percentage of male cells (*15*). The amount of donor myoblasts was measured on the day of MS implantation (n=5), 7 days (n=6), and 28 days (n=5) after implantation. Genomic DNA was prepared using an Allprep kit (Qiagen). Quantitative polymerase chain reaction of *sry* and *il2* was performed with 1.2 μg of DNA using Taqman universal polymerase chain reaction master mix (Applied Biosystems) according to the manufacturer's instructions and an ABI PRISM7700 sequence detection system (Applied Biosystems).

To evaluate the surviving engrafted cell histologically, five layers of MS made from myoblasts of GFP transgenic Lewis rats were implanted on the LV of Lewis rats. They were killed 28 days after the surgery.

Data Analysis

All data were expressed as the mean±standard error of mean and subjected to analysis of variance (ANOVA). Time-course data were first analyzed by using repeated-measurements two-way ANOVA, and the other numeric data were analyzed by using one-way ANOVA. If significance was found, posthoc comparisons were performed. Findings were considered significant at *P* less than 0.05.

REFERENCES

1. Dor V, Saab M, Coste P, et al. Left ventricular aneurysm: A new surgical approach. *Thorac Cardiovasc Surg* 1989; 37: 11.
2. Athanasuleus CL, Stanley AWH Jr, Buckberg GD. Restoration of contractile function in the enlarged left ventricle by exclusion of remodeled akinetic anterior segment: Surgical strategy, myocardial protection, and angiographic results. *J Card Surg* 1998; 13: 418.
3. Athanasuleus CL, Buckberg GD, Stanley AWH, et al. Surgical ventricular restoration in the treatment of congestive heart failure due to post-infarction ventricular dilation. *J Am Coll Cardiol* 2004; 44: 1439.
4. Menicanti L, Castelvecchio S, Ranucci M, et al. Surgical therapy for ischemic heart failure: Single-center experience with surgical anterior ventricular restoration. *J Thorac Cardiovasc Surg* 2007; 134: 433.
5. Jones RH, Velazquez EJ, Michler RE, et al. Coronary bypass surgery with or without surgical ventricular reconstruction. *N Engl J Med* 2009; 360: 1.
6. Dor V, Sabatier M, Di Donato M, et al. Efficacy of endoventricular patch plasty in large postinfarction akinetic scar and severe left ventricular dysfunction: Comparison with a series of large dyskinetic scars. *J Thorac Cardiovasc Surg* 1998; 116: 50.
7. Sinatra R, Macrina F, Braccio M, et al. Left ventricular aneurysmectomy; comparison between two techniques; early and late results. *Eur J Cardiothorac Surg* 1997; 12: 291.
8. Prucz RB, Weiss ES, Patel ND, et al. Coronary artery bypass grafting with or without surgical ventricular restoration: A comparison. *Ann Thorac Surg* 2008; 86: 806.
9. Taylor DA, Atkins BZ, Hungspreugs P, et al. Regenerating functional myocardium: Improved performance after skeletal myoblast transplantation. *Nat Med* 1998; 4: 929.
10. Orlic D, Kajstura J, Chiment S, et al. Bone marrow cells regenerate infracted myocardium. *Nature* 2001; 410: 701.
11. Memon IA, Sawa Y, Fukushima N, et al. Repair of impaired myocardium by means of implantation of engineered autologous myoblast sheets. *J Thorac Cardiovasc Surg* 2005; 130: 1333.
12. Kondoh H, Sawa Y, Miyagawa S, et al. Longer preservation of cardiac performance by sheet-shaped myoblast implantation in dilated cardiomyopathic hamsters. *Cardiovasc Res* 2006; 69: 466.

Copyright © 2012 Lippincott Williams & Wilkins. Unauthorized reproduction of this article is prohibited.

13. Hata H, Matsumiya G, Miyagawa S, et al. Grafted skeletal myoblast sheets attenuate myocardial remodeling in pacing-induced canine heart failure model. *J Thoracic Cardiovasc Surg* 2006; 132: 918.
14. Sekiya N, Matsumiya G, Miyagawa S, et al. Layered implantation of myoblast sheets attenuates adverse cardiac remodeling of the infracted heart. *J Thorac Cardiovasc Surg* 2009; 138: 985.
15. Kitagawa-Sakakida S, Tori M, Li Z, et al. Active cell migration in retransplanted rat cardiac allografts during the course of chronic rejection. *J Heart Lung Transplant* 2000; 19: 584.
16. Nishina T, Nishimura K, Yuasa S, et al. Initial effects of the left ventricular repair by placation may not last long in a rat ischemic cardiomyopathy model. *Circulation* 2001; 104: I-241.
17. Miyagawa S, Sawa Y, Taketani S, et al. Myocardial regeneration therapy for heart failure. Hepatocyte growth factor enhances the effect of cellular cardiomyoplasty. *Circulation* 2002; 105: 2556.
18. Shudo Y, Miyagawa S, Fukushima S, et al. Novel regenerative therapy using cell-sheet covered with omentum flap delivers a huge number of cells in a porcine myocardial infarction model. *J Thorac Cardiovasc Surg* 2011; 142: 1199.
19. Askari AT, Unzek S, Penn MMS, et al. Effect of stromal-cell-derived factor 1 on stem-cell homing and tissue regeneration in ischemic cardiomyopathy. *Lancet* 2003; 362: 97.
20. Miyagawa S, Roth M, Saito A, et al. Tissue-engineered cardiac constructs for cardiac repair. *Ann Thorac Surg* 2011; 91: 320.
21. Ratajczak MZ, Peier S, Janowska WA, et al. Expression of functional CXCR4 by muscle satellite cells and secretion of SDF-1 by muscle-derived fibroblasts is associated with the presence of both muscle progenitors in bone marrow and hematopoietic stem/progenitor cells in muscles. *Stem Cells* 2003; 21: 363.
22. Taniyama Y, Morishita R, Aoki M, et al. Angiogenesis and antifibrotic action by hepatocyte growth factor in cardiomyopathy. *Hypertension* 2002; 40: 47.
23. Shimizu T, Okamoto H, Chiba S, et al. VEGF-mediated angiogenesis is impaired by angiotensin type 1 receptor blockade in cardiomyopathic hamster hearts. *Cardiovasc Res* 2003; 58: 203.
24. Hoashi T, Matsumiya G, Miyagawa S, et al. Skeletal myoblast sheet transplantation improves the diastolic function of a pressure-overloaded right heart. *J Thorac Cardiovasc Surg* 2009; 138: 460.
25. Nakajima H, Nakajima HO, Salcher O, et al. Atrial but not ventricular fibrosis in mice expressing a mutant transforming growth factor-beta(1) transgene in the heart. *Circ Res* 2000; 86: 571.
26. Pokharel S, Rasoul S, Roks AJ, et al. *N*-acelyl-Ser-Asp-Lys-Pro inhibits phosphorylation of Smad2 in cardiac fibrosis. *Hypertension* 2002; 40: 155.
27. Oh J, Takahashi R, Kondo S, et al. The membrane-anchored MMP inhibitor RECK is a key regulator of extracellular matrix integrity and angiogenesis. *Cell* 2001; 107: 789.
28. Nomoto T, Nishina T, Miwa S, et al. Angiotensin-converting enzyme inhibitor helps prevent late remodeling after left ventricular aneurysm repair in rats. *Circulation* 2002; 106: I-115.
29. Kanemitsu H, Takai S, Tsuneyoshi H, et al. Chronic chymase inhibition preserves cardiac function after left ventricular repair in rats. *Eur J Cardiothorac Surg* 2008; 33: 25.
30. Sakakibara Y, Tambara K, Lu F, et al. Combined procedure of surgical repair and cell transplantation for left ventricular aneurysm: An experimental study. *Circulation* 2002; 106: I-193.
31. Sato T, Shishido T, Kawada T, et al. ESPVR of in situ rat left ventricle shows contractility-dependent curvilinearity. *Am J Physiol* 1998; 274: 1429.

Copyright © 2012 Lippincott Williams & Wilkins. Unauthorized reproduction of this article is prohibited.

Moriyama et al. BMC Cell Biology 2012, 13:21
http://www.biomedcentral.com/1471-2121/13/21

BMC Cell Biology

RESEARCH ARTICLE Open Access

Human adipose tissue-derived multilineage progenitor cells exposed to oxidative stress induce neurite outgrowth in PC12 cells through p38 MAPK signaling

Mariko Moriyama[1,2†], Hiroyuki Moriyama[1*†], Ayaka Ueda[1], Yusuke Nishibata[1], Hanayuki Okura[2], Akihiro Ichinose[3], Akifumi Matsuyama[2] and Takao Hayakawa[1]

Abstract

Background: Adipose tissues contain populations of pluripotent mesenchymal stem cells that also secrete various cytokines and growth factors to support repair of damaged tissues. In this study, we examined the role of oxidative stress on human adipose-derived multilineage progenitor cells (hADMPCs) in neurite outgrowth in cells of the rat pheochromocytoma cell line (PC12).

Results: We found that glutathione depletion in hADMPCs, caused by treatment with buthionine sulfoximine (BSO), resulted in the promotion of neurite outgrowth in PC12 cells through upregulation of bone morphogenetic protein 2 (BMP2) and fibroblast growth factor 2 (FGF2) transcription in, and secretion from, hADMPCs. Addition of *N*-acetylcysteine, a precursor of the intracellular antioxidant glutathione, suppressed the BSO-mediated upregulation of BMP2 and FGF2. Moreover, BSO treatment caused phosphorylation of p38 MAPK in hADMPCs. Inhibition of p38 MAPK was sufficient to suppress BMP2 and FGF2 expression, while this expression was significantly upregulated by overexpression of a constitutively active form of MKK6, which is an upstream molecule from p38 MAPK.

Conclusions: Our results clearly suggest that glutathione depletion, followed by accumulation of reactive oxygen species, stimulates the activation of p38 MAPK and subsequent expression of BMP2 and FGF2 in hADMPCs. Thus, transplantation of hADMPCs into neurodegenerative lesions such as stroke and Parkinson's disease, in which the transplanted hADMPCs are exposed to oxidative stress, can be the basis for simple and safe therapies.

Keywords: Human adipose-derived multilineage progenitor cells, Adult stem cells, Reactive oxygen species, p38 MAPK, Neurite outgrowth, BMP2, FGF2, Neurodegenerative disorders

Background

Mesenchymal stem cells (MSCs) are pluripotent stem cells that can differentiate into various types of cells [1-6]. These cells have been isolated from bone marrow [1], umbilical cord blood [2], and adipose tissue [3-6] and can be easily obtained and expanded *ex vivo* under appropriate culture conditions. Thus, MSCs are an attractive material for cell therapy and tissue engineering. Human adipose tissue-derived mesenchymal stem cells, also referred to as human adipose tissue-derived multilineage progenitor cells (hADMPCs), are especially advantageous because they can be easily and safely obtained from lipoaspirates, and the ethical issues surrounding other sources of stem cells can be avoided [4-6]. Moreover, hADMPCs have more pluripotent properties for regenerative medical applications than other stem cells, since these cells have been reported to have the ability to migrate to the injured area and differentiate into hepatocytes [4], cardiomyoblasts [5], pancreatic cells [7], and neuronal cells [8-10]. In addition, it is known that hADMPCs secrete a wide variety of cytokines and

* Correspondence: moriyama@phar.kindai.ac.jp
†Equal contributors
[1]Pharmaceutical Research and Technology Institute, Kinki University, 3-4-1 Kowakae, Higashi-Osaka, Osaka 577-8502, Japan
Full list of author information is available at the end of the article

BioMed Central

© 2012 Moriyama et al.; licensee BioMed Central Ltd. This is an Open Access article distributed under the terms of the Creative Commons Attribution License (http://creativecommons.org/licenses/by/2.0), which permits unrestricted use, distribution, and reproduction in any medium, provided the original work is properly cited.

growth factors necessary for tissue regeneration including nerve growth factor (NGF), brain-derived neurotrophic factor (BDNF), fibroblast growth factors (FGFs), vascular endothelial growth factor (VEGF) and hepatocyte growth factor (HGF) [11-14].

Recently, several groups have reported that hADMPCs facilitate neurological recovery in experimental models of stroke [9,10,15] and Parkinson's disease [16]. Despite the superiority of hADMPCs over other stem cells, the potential use of hADMPCs for the treatment of these neurodegenerative disorders has not been fully investigated. It has been reported that administration of hADMPCs in animal models of acute ischemic stroke markedly decreased brain infarct size, improved neurological function by enhancing angiogenesis and neurogenesis, and showed anti-inflammatory and anti-apoptotic effects [9,10]. These effects were due in part to increased secretion levels of VEGF, HGF and bFGF under hypoxic conditions [13], indicating the role of hADMPCs in reducing the severity of hypoxia-ischemic lesions.

In addition to hypoxic stress, ischemic lesions are generally subject to inflammation, which leads to the generation of reactive oxygen species (ROS) [17,18]. ROS are

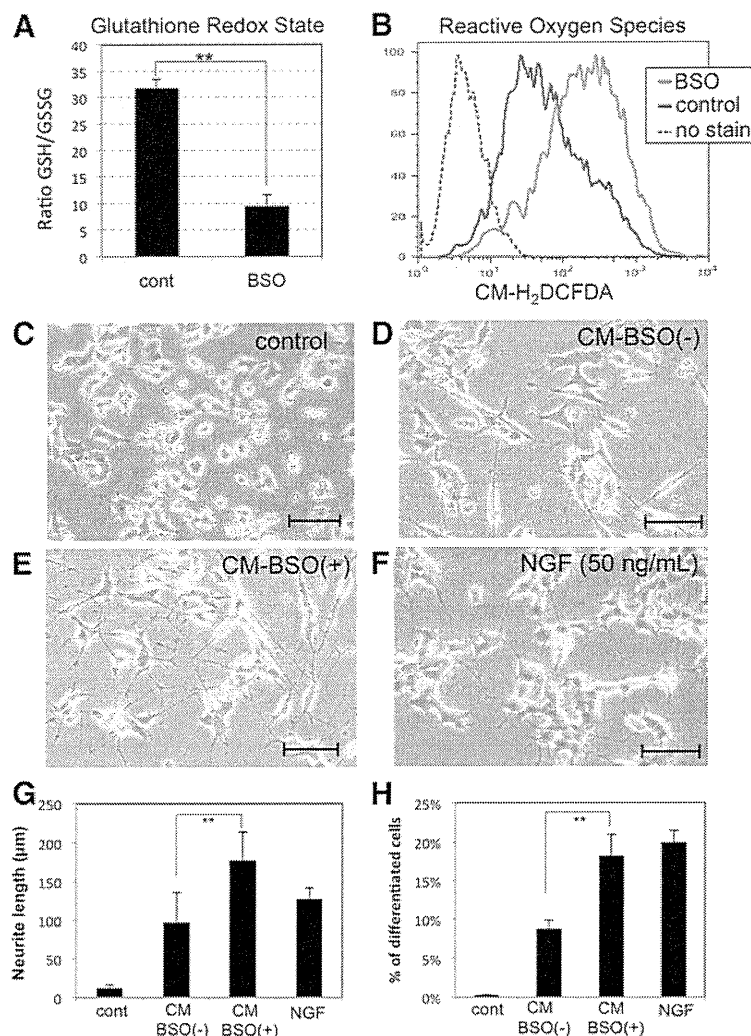

Figure 1 Conditioned medium from hADMPCs exposed to oxidative stress induces neurite outgrowth in PC12 cells. (A, B) Decrease of the reduced/oxidized glutathione ratios and increase in the intracellular ROS levels in hADMPCs treated with BSO. hADMPCs were treated with 1 mM BSO for 16 h, and cellular GSH/GSSG levels (**A**) or ROS (H_2O_2) levels (**B**) were analyzed. **(C-G)** Induction of neurite outgrowth in PC12 cells by conditioned medium from BSO-treated hADMPCs. PC12 cells were induced to differentiation by changing medium to differentiation medium alone (**C**), CM-BSO (–) (**D**), CM-BSO (+) (**E**), or differentiation medium with NGF (50 ng/mL) (**F**) for 2 days. Scale bars, 200 µm. (**G**) One hundred individual neurites were measured in each sample using Dynamic Cell Count Analyzer BZ-H1C (Keyence, Osaka, Japan) and average neurite length was calculated. **, P < 0.01 (Student's t test). **(H)** Percentage of neurite-bearing PC12 cells. A cell was scored positive for bearing neurites if it has a thin neurite extension that is double the length of the cell body diameter. A total of 500–600 cells in each sample were counted. **, P < 0.01 (Student's t test).

generated as a natural byproduct of normal aerobic metabolism, and mitochondrial respiration, together with oxidative enzymes such as plasma membrane oxidase, is considered to be the major intracellular source of ROS production [19]. Although appropriate levels of ROS play an important role in several physiological processes, oxidative damage initiated by excessive ROS causes many pathological conditions including inflammation, atherosclerosis, aging, and cancer. Neuronal cells are especially vulnerable to oxidative stress, and numerous studies have examined the crucial roles of oxidative stress in neurodegenerative disorders such as stroke [17,18], Alzheimer's disease [20,21], and Parkinson's disease [22,23]. In these diseases, microglia, the macrophages of the central nervous system (CNS), are activated in response to a local inflammation [24] and generate large amounts of reactive oxygen and nitrogen species, thereby exposing nearby neurons to stress [18,25]. Thus, the influence of oxidative stress generated by neurodegenerative lesion on hADMPCs needs to be further studied.

In this study, we examined the role of oxidative stress on hADMPCs in neurite outgrowth in cells of the rat pheochromocytoma cell line (PC12). Upon treatment with buthionine sulfoximine (BSO), an inhibitor of the rate-limiting enzyme in the synthesis of glutathione, hADMPCs accumulated ROS, which resulted in the upregulation of expression levels of the neurotrophic factors BMP2 and FGF2. Our present data thus provide new insights into understanding the mechanism of how hADMPCs exposed to oxidative stress contribute to neurogenesis, and this may explain the effects of stem cell transplantation therapy with hADMPCs in treating ischemic stroke.

Results

hADMPCs exposed to oxidative stress stimulate neurite outgrowth in PC12 cells

hADMPCs were treated with 1 mM BSO for 24 h; a group of hADMPCs that were not given any treatment was used as the control group. As shown in Figure 1A and B, BSO treatment resulted in significant reduction of intracellular reduced glutathione levels, followed by accumulation of intracellular reactive oxygen species (ROS) in hADMPCs. To investigate whether accumulation of ROS affects secretion of cytokines from hADMPCs, conditioned medium from BSO-treated (CM-BSO (+)) or BSO-untreated (CM-BSO (−)) hADMPCs was added to PC12 cells. As expected, addition of NGF significantly induced neurite outgrowth in the PC12 cells (Figure 1F, G, H). hADMPCs, like other mesenchymal stem cells derived from bone marrow or adipose tissue, may secrete many cytokines including NGF, BDNF and FGF2, and this may account for the slight induction of neurite outgrowth seen in the CM-BSO (−) treated cells (Figure 1D, G, H). In contrast, the number and length of neurite outgrowth of PC12 cells in CM-BSO (+) (Figure 1E) was markedly enhanced compared with those in CM-BSO (−) (Figure 1D, E, G, H).

Conditioned medium from BSO-treated hADMPCs activates Erk1/2 MAPK and Smad signaling in PC12 cells

To investigate which intracellular signaling pathways were involved in the neurite outgrowth of PC12 cells in CM-BSO (+), we used western blotting to determine the phosphorylation levels of Erk1/2 MAPK, p38 MAPK, Smad1/5/8 and Akt in PC12 cells in various culture conditions. NGF significantly activated Erk1/2 MAPK and Akt signaling pathway (Figure 2). In contrast, Erk1/2 MAPK was not activated in PC12 cells exposed to CM-BSO (−), while an increase in phosphorylated Smad1/5/8 was observed. Interestingly, CM-BSO (+) treatment led to both a significant increase in Smad1/5/8 phosphorylation levels as well as activation of the Erk1/2 MAPK

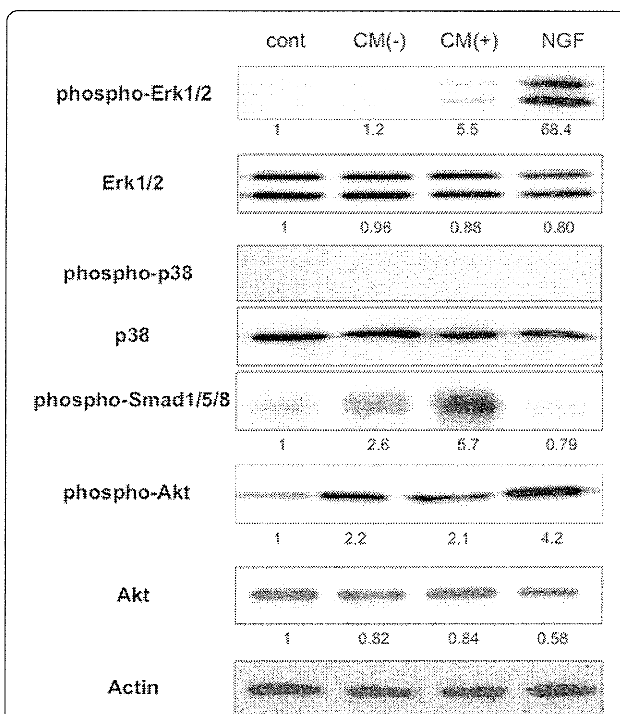

Figure 2 Erk1/2 MAPK and Smad1/5/8 are activated in PC12 cells cultured in conditioned medium from BSO-treated hADMPCs. Western blot analysis of PC12 cells cultured in differentiation medium alone (cont), CM-BSO (−), CM-BSO (+), or differentiation medium with NGF (50 ng/mL) for 1 h. Proteins extracted from each cell culture were resolved by SDS-PAGE, transferred to a membrane, and probed with anti-phosphorylated Erk1/2 (phospho Erk1/2), anti-Erk1/2, anti-phosphorylated p38 (phospho p38), anti-p38, anti-phosphorylated Smad1/5/8 (phospho Smad1/5/8), anti-phosphorylated Akt (phospho Ark) and anti-Akt. Actin was analyzed as an internal control. Numbers below blots indicate relative band intensities as determined by the ImageJ software.

signaling pathway in PC12 cells (Figure 2). Akt was 2-fold activated in both CM-BSO (−) and CM-BSO (+) treated PC12 cells, but no significant difference between the 2 groups was observed.

FGF2 and BMP2 are upregulated through p38 MAPK signaling in hADMPCs exposed to oxidative stress

We next examined which growth factors or cytokines from BSO-treated hADMPCs were involved in stimulation of neurite outgrowth. We found that both mRNA (Figure 3A and B) and protein (Figure 3C and D) levels for BMP2 and FGF2 were markedly increased in hADMPCs treated with BSO. To determine if this upregulation was caused by ROS, all cells were exposed to the antioxidant *N*-acetylcysteine (NAC). As we expected, addition of NAC to BSO-treated hADMPCs reduced the expression levels of BMP2 and FGF2 to control levels (Figure 3E and F). As BMP2 together with FGF2 has

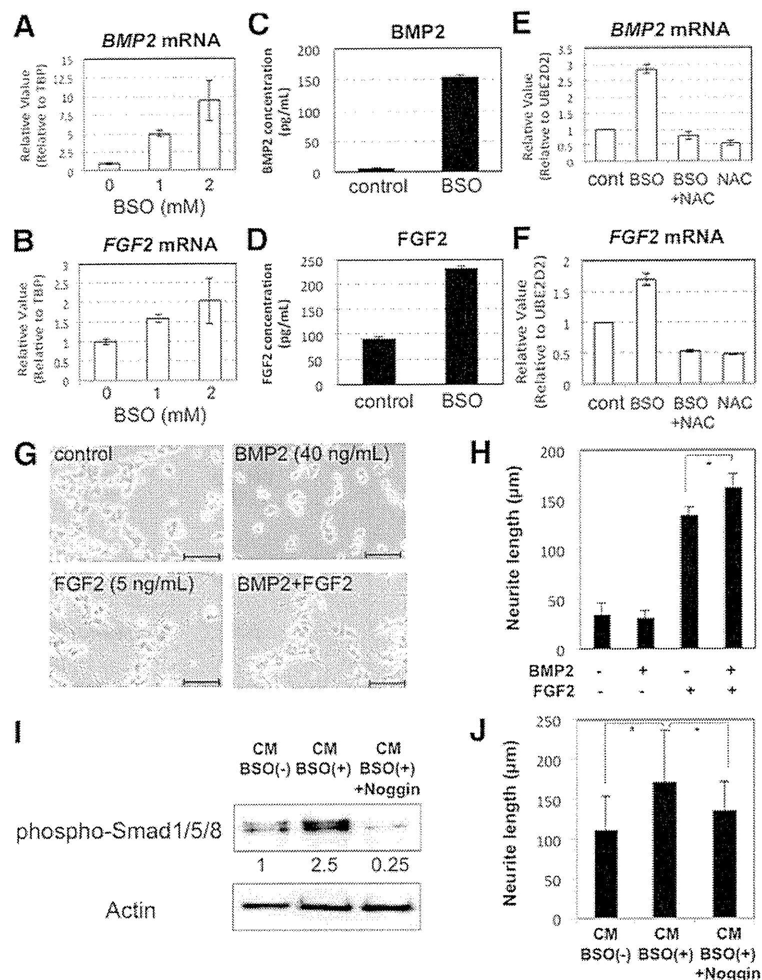

Figure 3 Transcription and secretion of BMP2 and FGF2 were increased in hADMPCs exposed to oxidative stress. (A, B) Upregulation of *BMP2* (**A**) and *FGF2* (**B**) mRNA in hADMPCs by BSO in a dose-dependent manner. **(C, D)** Secretion of BMP2 (**C**) and FGF2 (**D**) from hADMPCs in medium alone (cont) or with addition of 1 mM BSO (BSO) was analyzed by ELISA. **(E, F)** NAC treatment repressed the expression levels of *BMP2* and *FGF2* upregulated by BSO to the control levels. Expression of *BMP2* (E) and *FGF2* (F) mRNA was analyzed by q-PCR. cDNA was generated from total RNA extracted from hADMPCs (cont), hADMPCs treated with 1 mM BSO (BSO), 1 mM BSO + 5 mM NAC (BSO + NAC), and 5 mM NAC (NAC). The most reliable internal control gene was determined using the geNorm Software. **(G, H)** PC12 cells were cultured in differentiation medium alone (control), or differentiation medium supplemented with BMP2 (40 ng/mL), FGF2 (5 ng/mL), or both BMP2 and FGF2 (BMP2 + FGF2) for 2 days. (**G**) Representative images of neurite outgrowth in PC12 cells. Scale bars, 200 μm. (**H**) One hundred individual neurites were measured in each sample using Dynamic Cell Count Analyzer BZ-H1C (Keyence) and average neurite length was calculated. *, $P < 0.05$ (Student's t test). **(I, J)** PC12 cells were cultured in CM-BSO (−), CM-BSO (+), or CM-BSO (+) added with recombinant murine Noggin (200 ng/mL). **(I)** Western blot analysis of PC12 cells 1 h after CM treatment. Proteins extracted from each sample were resolved by SDS-PAGE, transferred to a membrane, and probed with anti-phosphorylated Smad1/5/8 (phospho-Smad1/5/8) and anti-Actin. Numbers below blots indicate relative band intensities as determined by the ImageJ software. (**J**) Two days after CM treatment, 100 individual neurites in PC12 cells were measured in each sample using Dynamic Cell Count Analyzer BZ-H1C (Keyence) and average neurite length was calculated. *, $P < 0.05$ (Student's t test).

previously been shown to induce neurite outgrowth in PC12 cells [26,27], we examined the effect of BMP2 and FGF2 on neurite outgrowth. We confirmed that PC12 cells did not differentiate effectively by BMP2 treatment alone, but BMP2 significantly augmented FGF2-induced neurite outgrowth in PC12 cells (Figure 3G and H), as previously reported. Moreover, in order to confirm the effect of BMP2 on neurite outgrowth in PC12 cells, 200 ng/mL of Noggin, an antagonist of BMP signaling, was added to CM-BSO(+). Addition of Noggin significantly suppressed the CM-BSO (+)-evoked phosphorylation of Smad1/5/8 (Figure 3I) and shortened the length of neurite outgrowth in PC12 cells (Figure 3J).

To address the question of which intracellular signaling pathways are affected by oxidative stress in hADMPCs, we focused on MAPK signaling since previous studies had suggested that accumulation of ROS in cells led to the activation of Erk1/2, p38, and JNK MAPK [28,29]. Western blotting revealed that BSO treatment markedly activated the p38 MAPK pathway; SB203580 could inhibit the activation, and U0126 treatment stimulated the activation (Figure 4A). ERK1/2 MAPK was significantly phosphorylated by BSO treatment, and ERK1/2 activation was reduced to the control level by treatment with U0126 (Figure 4B). In contrast, JNK activation was not observed in BSO-treated hADMPCs (Figure 4B). Therefore, we further investigated the relationship between increases in BMP2 and FGF2 expression and activation of the p38 and ERK1/2 MAPK signaling pathways by oxidative stress. Treatment

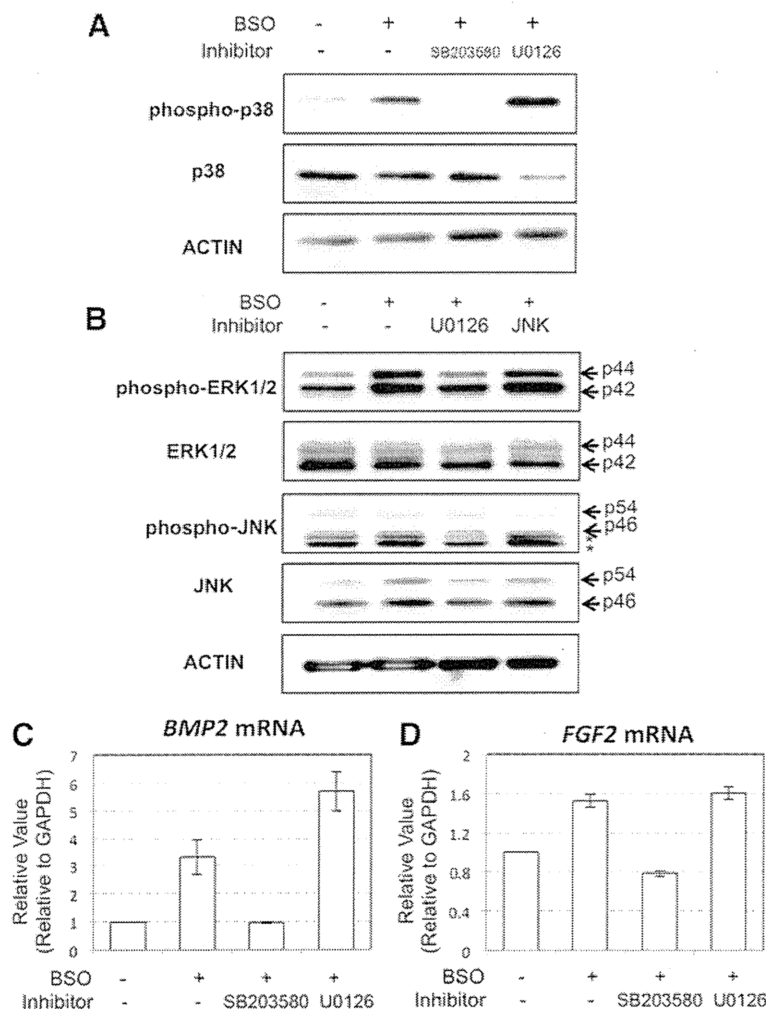

Figure 4 BMP2 and FGF2 were upregulated through activation of p38 MAPK. Inhibiton of p38 MAPK resulted in the supression of *BMP2* and *FGF2* transcripts upregulated by BSO treatment in hADMPCs. hADMPCs were pre-treated with 10 μM of SB203580, 10 μM of U0126 or 10 μM of JNK inhibitor II for 2 h followed by 1 mM BSO treatment for 16 h. The medium was replaced with fresh culture medium and the cells were cultured for another 2 days. **(A)** Western blot analysis of p38 MAPK activation in hADMPCs. **(B)** Western blot analysis of ERK1/2 MAPK, JNK SAPK activation in hADMPCs. **(C, D)** Transcription levels of *BMP2* (**C**) and *FGF2* (**D**) were analyzed by q-PCR. The most reliable internal control gene was determined using the geNorm Software.

with the p38 MAPK inhibitor SB203580 dramatically downregulated the expression levels of *BMP2* and *FGF2* to control levels (Figure 4C and D). In contrast, the Erk1/2 MAPK inhibitor U0126 had no effect on *FGF2* expression levels and led to a slight increase in *BMP2* expression (Figure 4C and D).

MKK6-mediated activation of p38 MAPK increases BMP2 and FGF2 expression in hADMPCs

To further confirm the involvement of p38 MAPK in the regulation of BMP2 and FGF2, hADMPCs were transduced with a lentiviral vector expressing constitutively active MKK6 (MKK6 (glu)) [30] from an EF1α promoter. As shown in Figure 5A, lentiviral transduction of MKK6 (glu) led to expression of Flag-tagged MKK6 (glu) in hADMPCs. Moreover, the expression of MKK6 (glu) resulted in activation of p38 MAPK as expected [30] (Figure 5A), and upregulation of BMP2 and FGF2 expression (Figure 5B-E).

NF-κB is not activated in hADMPCs exposed to oxidative stress

It has been reported that NF-κB directly binds to the *BMP2* promoter to induce its expression [31], and MSK1, a downstream molecule of p38 MAPK, is involved in NF-κB transactivation [32]. Therefore, we

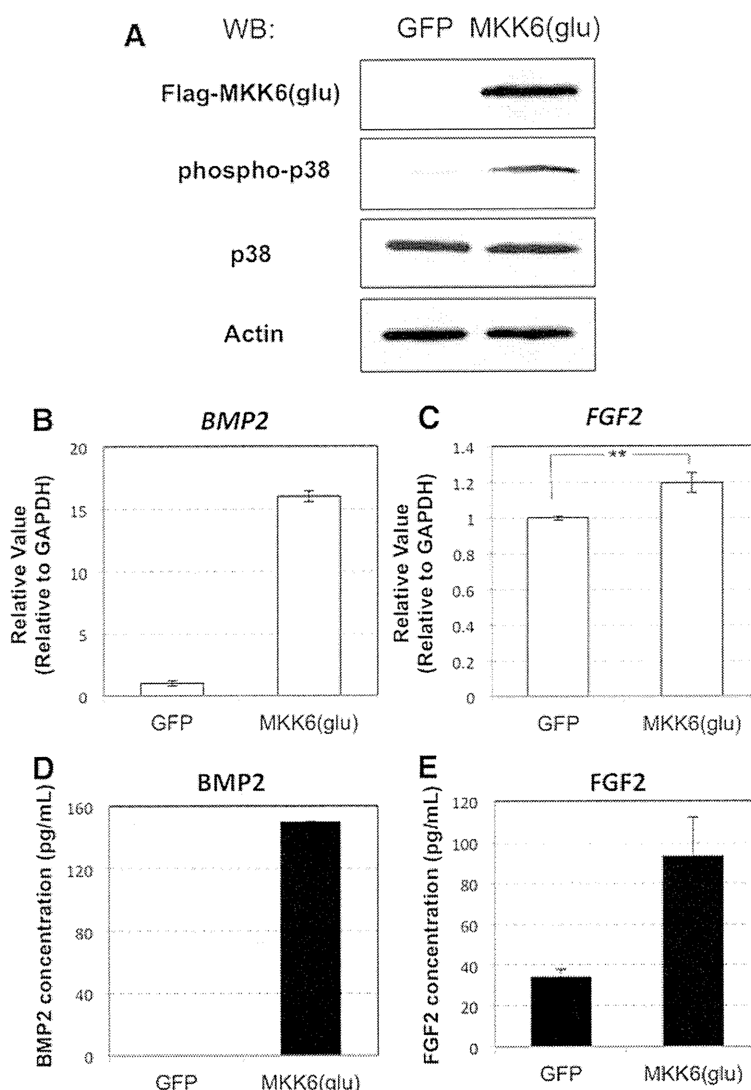

Figure 5 Activation of p38 MAPK by a constitutively active form of MKK6 resulted in elevated expression of BMP2 and FGF2. (A) A lentiviral vector expressing Flag-tagged MKK6 (glu) was transfected into hADMPCs. Expression of Flag-tagged MKK6 (glu), phosphorylated p38 MAPK and p38 MAPK was analyzed by western blotting. A CSII-EF-EGFP lentiviral vector was infected as a control (GFP). Actin was detected as an internal control. **(B, C)** Transcriptional levels of *BMP2* **(B)** and *FGF2* **(C)** were analyzed by q-PCR. The most reliable internal control gene was determined using the geNorm Software. **(D, E)** BMP2 **(D)** and FGF2 **(E)** secretion was analyzed by ELISA.

hypothesized that p38 MAPK-mediated activation of NF-κB might contribute to elevated expression of *BMP2* mRNA. To confirm this hypothesis, transcriptional activation of NF-κB was examined by measuring luciferase activity driven by the synthetic NF-κB response element. We found that transcriptional activity of NF-κB was not stimulated by BSO treatment (Figure 6A), and immunocytochemical analysis also revealed that NF-κB was not activated (nuclear localization of NF-κB/p65 was rarely observed) in BSO-treated hADMPCs (Figure 6B). These results suggested that elevated expression of *BMP2* mRNA is not mediated by NF-κB signaling.

Our current data thus demonstrate the crucial role of ROS, via activation of the p38 MAPK signaling pathway, in regulating expression levels of the neurotrophic factors BMP2 and FGF2 in hADMPCs. The overall model that we propose, based upon our findings, is shown in Figure 7.

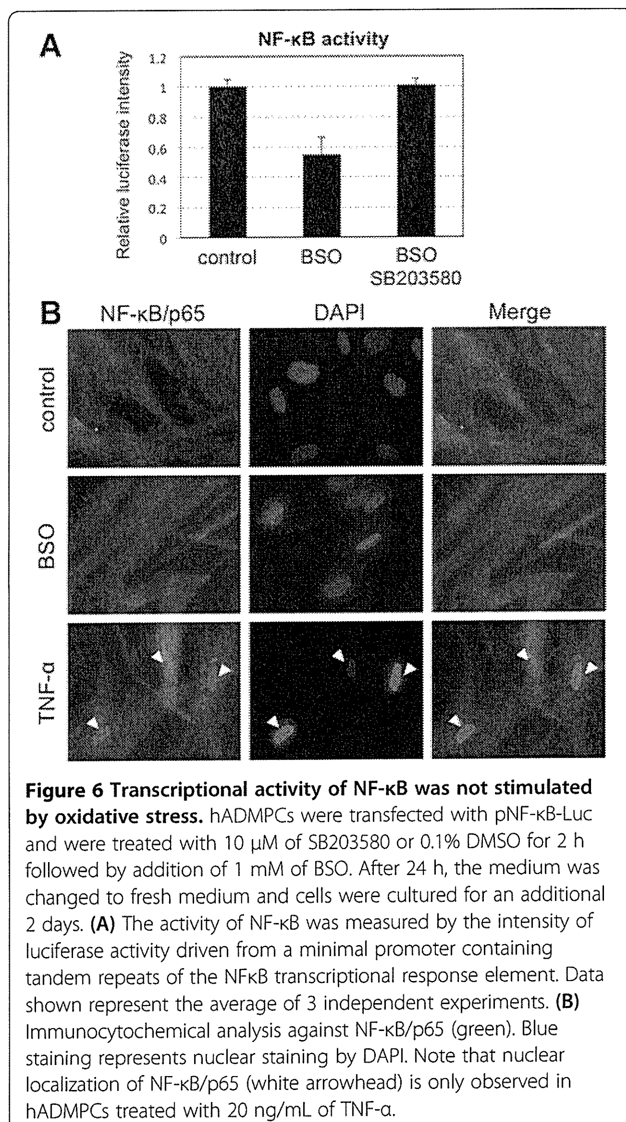

Figure 6 Transcriptional activity of NF-κB was not stimulated by oxidative stress. hADMPCs were transfected with pNF-κB-Luc and were treated with 10 μM of SB203580 or 0.1% DMSO for 2 h followed by addition of 1 mM of BSO. After 24 h, the medium was changed to fresh medium and cells were cultured for an additional 2 days. **(A)** The activity of NF-κB was measured by the intensity of luciferase activity driven from a minimal promoter containing tandem repeats of the NFκB transcriptional response element. Data shown represent the average of 3 independent experiments. **(B)** Immunocytochemical analysis against NF-κB/p65 (green). Blue staining represents nuclear staining by DAPI. Note that nuclear localization of NF-κB/p65 (white arrowhead) is only observed in hADMPCs treated with 20 ng/mL of TNF-α.

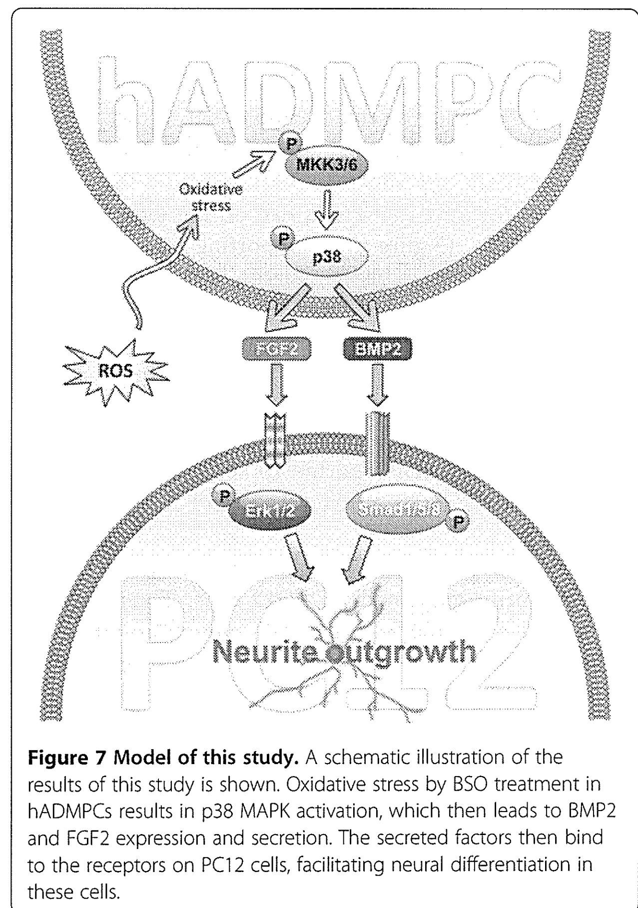

Figure 7 Model of this study. A schematic illustration of the results of this study is shown. Oxidative stress by BSO treatment in hADMPCs results in p38 MAPK activation, which then leads to BMP2 and FGF2 expression and secretion. The secreted factors then bind to the receptors on PC12 cells, facilitating neural differentiation in these cells.

Discussion

In this study, we investigated the effect of oxidative stress in hADMPCs on the induction of neuronal differentiation. Such mechanisms may explain how administration of hADMPCs to neurodegenerative lesions enhances endogenous repair mechanisms via neurogenesis of endogenous neural progenitor and stem cells. Damaged tissues, such as the brain tissue of patients who have suffered from ischemic stroke, are subject to inflammation and the generation of reactive oxygen species (ROS) [17,18]. Our data demonstrated that hADMPCs, when exposed to oxidative stress, facilitate neuronal differentiation in rat pheochromocytoma cell line PC12 cells by upregulation of fibroblast growth factor 2 (FGF2) and bone morphogenetic protein 2 (BMP2) secretion through p38 MAPK activation.

Our results show that BMP2 and FGF2 were upregulated in hADMPCs when exposed to buthionine sulfoximine (BSO), a glutathione-synthesis inhibitor that leads to oxidative stress. These findings may have therapeutic implications in neurodegenerative diseases. We concluded that BMP2 and FGF2 secreted from hADMPCs that had been exposed to oxidative stress were the main inducers of neurite outgrowth in PC12 cells. Erk1/2 and

Smad1/5/8 were significantly activated in these cells (Figure 2), while other growth factors known to induce neurite outgrowth in PC12 cells such as nerve growth factor (NGF) and vascular endothelial growth factor (VEGF) were not observed to be upregulated by BSO treatment (data not shown). We confirmed that BMP2 enhanced the effect that FGF2 had on the differentiation of PC12 cells (Figure 3), supporting our idea that hADMPCs under oxidative stress conditions secrete BMP2 and FGF2 and that this contributes to neuronal differentiation. Consistent with our conclusions, it has been reported that BMP2, via activation of a Smad signaling pathway, facilitated FGF2-induced neuronal differentiation in PC12 cells [26,27]. However, since hADMPCs have been reported to secrete many growth factor including NGF, VEGF, HGF, and IGF [11,15,33], we cannot exclude the possibility that BMP2 and FGF2 are acting cooperatively with these growth factors to facilitate neurite outgrowth in PC12 cells. Thus, the precise molecular mechanisms of induction of PC12 differentiation and the precise expression profiles in BSO-treated hADMPCs need to be further investigated.

Recently, BMP signaling through Smad1/5/8 has been reported to contribute to neurite outgrowth in dorsal root ganglion neurons both in vitro and in vivo [34,35]. Moreover, BMP2 has been shown to have neurotrophic effects on midbrain dopaminergic neurons [36], ventral mesencephalic neurons [37], mouse embryonic striatal neurons [38], and nitrergic and catecholaminergic enteric neurons [39]. Moreover, FGF2 is trophic for neurons, glias, and endothelial cells in the central nervous system. FGF2 also prevents downregulation of the anti-apoptotic protein Bcl-2 in ischemic brain tissue and limits excitotoxic damage to the brain through an activin-dependent mechanism [40]. These findings are consistent with our hypothesis that hADMPCs secret BMP2 and FGF2 to induce neurogenesis in neurodegenerative lesions in response to oxidative stress.

As it has been shown that ROS activate ERKs, JNKs, and p38 MAPKs [28,29], we examined the MAPK signaling pathway in hADMPCs exposed to oxidative stress and found that BSO treatment resulted in significant activation of ERK1/2 and p38 MAPK. Intriguingly, addition of SB203580, a specific inhibitor of p38 MAPK, but not the ERK inhibitor U0126, suppressed *BMP2* and *FGF2* expression in BSO-treated hADMPCs to control levels (Figure 4), suggesting that p38 MAPK was contributing to upregulation of BMP2 and FGF2 in hADMPCs when exposed to oxidative stress. Moreover, lentiviral transduction of the constitutively active form of MKK6, a MAPKK that selectively activates p38 MAPK isoforms [30], resulted in upregulation of BMP2 and FGF2 and this also demonstrated the crucial role of the p38 MAPK cascade in the regulation of BMP2 and FGF2. In primary human endothelial cells, p38-dependent regulation of BMP2 expression was reported previously. Viemann *et al.* [41] investigated the genes that were induced by inflammatory stimulation with tumor necrosis factor α (TNF-α) and classified these genes into 2 categories based on whether they were regulated in an NF-κB-dependent or p38 MAPK-dependent manner. Consistent with our findings, they found that significant induction of BMP2 expression by TNF-α was markedly suppressed by SB202190, an inhibitor of p38 MAPK. These results support the hypothesis that activation of the p38 MAPK pathway in hADMPCs in response to inflammation surrounding neurodegenerative lesions leads to induction of BMP2 and FGF2, which in turn support regeneration of neuronal cells.

It has been known that NF-κB directly binds to the BMP2 promoter to induce its expression [31], and MSK1, a downstream molecule of p38 MAPK, is involved in NF-κB transactivation [32]. However, we did not observe an elevation of NF-κB transcriptional activity in hADMPCs when they were exposed to oxidative stress (Figure 6). The mechanism of p38-dependent regulation of gene expression is not completely understood, and the precise mechanism by which p38 MAPK regulates the expression of BMP2 and FGF2 remains to be determined.

In this study, we also found that suppression of ERK1/2 MAPK by U0126 in BSO-treated hADMPCs resulted in slight activation of p38 MAPK (Figure 4A). Consistent with this, the expression level of *BMP2* mRNA was also upregulated when cells exposed to oxidative stress were pretreated with U0126 (Figure 4C). Previously, "seesaw cross-talk" between ERK and p38 MAPK signaling has been reported; i.e., the MEK inhibitor caused a decrease in the phosphorylation level of ERK and an increase in that of p38, whereas the p38 inhibitor had the opposite effect [42-44]. We did not investigate the phosphorylation of ERK1/2 in SB203580-treated hADMPCs, but it may be possible that seesaw cross-talk also occurs in our system.

Conclusions

In summary, the results obtained in this study have demonstrated the potential use of hADMPCs for the treatment of neurodegenerative diseases such as ischemic stroke, Parkinson's disease, Alzheimer's disease, and spinal cord injury, in which the transplanted hADMPCs might be exposed to oxidative stress. Moreover, the p38-dependent modulation of BMP2 and FGF2 expression observed in this study is expected to be a new therapeutic target for neurodegenerative disorders.

Materials and methods

Adipose tissue samples

Subcutaneous adipose tissue samples (10–50 g, each) were resected during plastic surgery in 5 females (age,

20–60 years) as excess discards. The study protocol was approved by the Review Board for Human Research of Kobe University Graduate School of Medicine, Foundation for Biomedical Research and Innovation and Kinki University Pharmaceutical Research and Technology Institute (reference number: 10–005). Each subject provided a signed informed consent.

Cell culture

PC12 cells were obtained from the Health Science Research Resources Bank (Osaka, Japan) and maintained in RPMI1640 media supplemented with 10% heat-inactivated horse serum and 5% fetal bovine serum. For differentiation, the cells were plated in 6-well culture plates coated with collagen type I (Nitta Gelatin, Osaka, Japan) and the medium was replaced with differentiation medium (RPMI1640 supplemented with 1% horse serum and 0.5% fetal bovine serum) or conditioned medium from hADMPCs. NGF (50 ng/mL), BMP2 (40 ng/mL) or FGF2 (5 ng/mL) were added to the differentiation medium. Recombinant murine Noggin (200 ng/mL: PeproTech, NJ, USA) was added to conditioned medium from BSO-treated hADMPCs. hADMPCs were isolated as previously reported [4-6,45,46] and maintained in a medium containing 60% DMEM-low glucose, 40% MCDB-201 medium (Sigma Aldrich, St. Louis, MO, USA), 1× insulin-transferrin-selenium (Gibco Invitrogen, NY, USA), 1 nM dexamethasone (Sigma Aldrich), 100 mM ascorbic acid 2-phosphate (Wako, Osaka, Japan), 10 ng/mL epidermal growth factor (PeproTech), and 5% fetal bovine serum. The cells were plated to a density of 5×10^3 cells/cm^2 on fibronectin-coated dishes, and the medium was replaced every 2 days.

Preparation of conditioned medium from hADMPCs

Two days after plating, hADMPCs were treated with BSO (concentrations used were varied in each experiment and are indicated in the results and figure legends) for 16 h. The medium was replaced with fresh culture medium for 2 days followed by replacement with PC12 cell differentiation medium. After 2 more days, the medium was removed for use as conditioned medium. For preparation of the conditioned medium from hADMPCs in which one of the three, p38, Erk1/2, or JNK MAPK, was inhibited, hADMPCs were pretreated with 10 μM SB203580 (Promega, WI, USA), 10 μM U0126 (Promega), or 10 μM JNK inhibitor II (EMD4 Bioscience, CA, USA), respectively, for 2 h and subsequently treated with 1 mM BSO.

Measurement of GSH/GSSG ratio

Ratios of reduced glutathione (GSH) to oxidized glutathione (GSSG) were measured using the GSH/GSSG-Glo assay kit (Promega) following the manufacturer's protocol.

Measurement of reactive oxygen species production

Cells were harvested and incubated with 10 μM 5-(and-6)-chloromethyl-2′,7′-dichlorodihydrofluorescein diacetate, acetyl ester (CM-H_2DCFDA). The amount of intracellular ROS production was proportional to green fluorescence, as analyzed with a Guava easyCyte 8HT flow cytometer (Millipore) using an argon laser at 488 nm and a 525/30 nm band pass filter, and dead cells were excluded with the LIVE/DEAD fixable far red dead cell stain kit (Invitrogen).

Western blot analysis

Cells were washed with ice-cold phosphate-buffered saline and lysed with M-PER Mammalian Protein Extraction Reagent (Thermo Scientific Pierce, IL, USA) following the manufacturer's instructions. Equal amounts of proteins were separated by sodium dodecylsulfate polyacrylamide gel electrophoresis (SDS-PAGE), transferred to polyvinylidene fluoride (PVDF) membranes (Immobilon-P; Millipore, MA, USA), and probed with antibodies against phospho-Erk1/2 (#4370), Erk1/2 (#4695), phospho-38 (#9215), p38 (#9212), phospho-Smad1/5/8 (#9511), phospho-Akt (#4060), Akt (#4691), phospho-JNK (#9251), JNK (#9258) (all from Cell Signaling Technology, MA, USA) and actin (Millipore). Horseradish peroxidase (HRP)-conjugated anti-rabbit and anti-mouse secondary antibodies (Cell Signaling Technology, Danvers, MA, USA) were used as probes and immunoreactive bands were visualized with the Immobilon Western Chemiluminescent HRP substrate (Millipore). The band intensity was measured using ImageJ software.

RNA extraction, cDNA generation, and quantitative polymerase chain reaction (q-PCR)

Total RNA was extracted using the RNeasy Mini Kit (Qiagen, Hilden, Germany) following the manufacturer's instructions. cDNA was generated from 1 μg of total RNA using the Verso cDNA Synthesis Kit (Thermo Scientific) and purified with the MinElute PCR Purification Kit (Qiagen). Q-PCR analysis was carried out using the SsoFast EvaGreen supermix (Bio-Rad, CA, USA) according to the manufacturer's protocols. The relative expression value of each gene was calculated using a ΔΔCt method and the most reliable internal control gene was determined using the geNorm Software (http://medgen.ugent.be/~jvdesomp/genorm/). Details of the primers used in these experiments are available on request.

Enzyme-linked immunosorbent assay

Enzyme-linked immunosorbent assay (ELISA) was performed using the Quantikine BMP-2 Immunoassay System and Quantikine FGF-2 Immunoassay System (R&D

Systems, MN, USA) following the manufacturer's protocols.

Plasmid construction and lentivirus production

Flag-tagged MKK6 (glu) [30] was provided by Addgene (pcDNA3-Flag MKK6 (glu); Addgene plasmid 13518). Flag-tagged MKK6 (glu) was cloned into a pENTR11 vector (Invitrogen). An iresGFP fragment was subsequently cloned into the plasmid to produce the entry vector pENTR11-MKK6 (glu)-iresGFP. The entry vector and CSII-EF-RfA (kindly provided by Dr. Miyoshi, RIKEN BioResource Center, Tsukuba, Japan) were incubated with LR clonase II enzyme mix (Invitrogen) to generate CSII-EF-MKK6 (glu)-iresGFP. The resultant plasmid was mixed with packaging plasmids (pCAG-HIVg/p and pCMV-VSVG-RSV-Rev, kindly provided by Dr. Miyoshi) and transfected into 293 T cells. The supernatant medium, which contained lentiviral vectors, was collected 2 days after transduction and concentrated by centrifugation (6000 G, 15 h, 4°C).

Luciferase assay

hADMPCs were transfected with pGL4.74 (Promega) and either pTAL-Luc or pNF-κB-Luc by TransIT-2020 (TaKaRa-Bio). The cells were then treated with 10 μM of SB203580 or 0.1% DMSO for 2 h followed by addition of 1 mM of BSO. After 24 h, the medium was changed to fresh medium and cells were cultured for an additional 2 days. The activity of NF-κB was measured using the Dual Luciferases Assay System (Promega) according to the manufacturer's protocol.

Immunocytochemistry

hADMPCs were fixed with 4% paraformaldehyde in PBS for 10 min at 4°C and then washed 3 times in PBS. Blocking was performed with PBSMT (PBS containing 0.1% Triton X-100, 2% Skim Milk) for 1 h at room temperature. The cells were then incubated with rabbit monoclonal antibody against NF-κB p65 (Cell Signaling; #8242; 1/100 dilution) overnight at 4°C. After washing with PBS, cells were incubated with Alexa 488 conjugated anti-rabbit IgG (Invitrogen; 1/1000 dilution) for 1 h. The cells were counterstained with 4′-6-diamidino-2-phenylindole (DAPI) (Invitrogen) to identify cellular nuclei.

Competing interests

None of the authors have any competing interests related to the manuscript.

Authors' contributions

MM carried out the FACS analysis, qPCR analysis, ELISA, immunofluorescent staining, and cell culture, participated in the study design, and drafted the manuscript. HM participated in the study design, carried out the western blot analysis, luciferase assay, and cell culture, and drafted the manuscript. AU carried out western blot analysis, constructed the plasmids, and generated the lentiviral vectors. YN carried out qPCR analysis and performed the statistical analysis. AI resected subcutaneous adipose tissue samples during plastic surgery. HO and AM isolated hADMPCs from human adipose tissues. TH conceived the study, participated in its design and coordination, and helped to draft the manuscript. All authors read and approved the final manuscript.

Acknowledgements

We thank A Nishikawa, T Fukase, T Sasaki, T Shoji, K Nakagita, S Fukui, and K Honjo for technical support. We thank Dr. Roger Davis for providing the pcDNA3-Flag MKK6 (glu) plasmid and Dr. Hiroyuki Miyoshi for the CSII-EF-RfA, pCMV-VSVG-RSV-Rev and pCMV-HIVg/p plasmids. This work was supported in part by grants from the Ministry of Health, Labor, and Welfare of Japan and a grant from the Program for Promotion of Fundamental Studies in Health Sciences of the National Institute of Biomedical Innovation (NIBIO).

Author details

[1]Pharmaceutical Research and Technology Institute, Kinki University, 3-4-1 Kowakae, Higashi-Osaka, Osaka 577-8502, Japan. [2]Department of Somatic Stem Cell Therapy and Health Policy, Foundation for Biomedical Research and Innovation, TRI305, 1-5-4 Minatojima-minamimachi, Chuo-ku, Kobe, Hyogo 650-0047, Japan. [3]Department of Plastic Surgery, Kobe University Hospital, Kobe, Japan.

Received: 28 March 2012 Accepted: 2 August 2012
Published: 7 August 2012

References

1. Pittenger MF, Mackay AM, Beck SC, Jaiswal RK, Douglas R, Mosca JD, Moorman MA, Simonetti DW, Craig S, Marshak DR: **Multilineage potential of adult human mesenchymal stem cells.** *Science* 1999, **284**:143–147.
2. Bieback K, Kern S, Kluter H, Eichler H: **Critical parameters for the isolation of mesenchymal stem cells from umbilical cord blood.** *Stem Cells* 2004, **22**:625–634.
3. Zuk PA, Zhu M, Ashjian P, De Ugarte DA, Huang JI, Mizuno H, Alfonso ZC, Fraser JK, Benhaim P, Hedrick MH: **Human adipose tissue is a source of multipotent stem cells.** *Mol Biol Cell* 2002, **13**:4279–4295.
4. Okura H, Komoda H, Saga A, Kakuta-Yamamoto A, Hamada Y, Fumimoto Y, Lee CM, Ichinose A, Sawa Y, Matsuyama A: **Properties of hepatocyte-like cell clusters from human adipose tissue-derived mesenchymal stem cells.** *Tissue Eng Part C Methods* 2010, **16**:761–770.
5. Okura H, Matsuyama A, Lee CM, Saga A, Kakuta-Yamamoto A, Nagao A, Sougawa N, Sekiya N, Takekita K, Shudo Y, *et al*: **Cardiomyoblast-like cells differentiated from human adipose tissue-derived mesenchymal stem cells improve left ventricular dysfunction and survival in a rat myocardial infarction model.** *Tissue Eng Part C Methods* 2010, **16**:417–425.
6. Komoda H, Okura H, Lee CM, Sougawa N, Iwayama T, Hashikawa T, Saga A, Yamamoto-Kakuta A, Ichinose A, Murakami S, Sawa Y, Matsuyama A: **Reduction of N-glycolylneuraminic acid xenoantigen on human adipose tissue-derived stromal cells/mesenchymal stem cells leads to safer and more useful cell sources for various stem cell therapies.** *Tissue Eng Part A* 2010, **16**:1143–1155.
7. Okura H, Komoda H, Fumimoto Y, Lee CM, Nishida T, Sawa Y, Matsuyama A: **Transdifferentiation of human adipose tissue-derived stromal cells into insulin-producing clusters.** *J Artif Organs* 2009, **12**:123–130.
8. Safford KM, Safford SD, Gimble JM, Shetty AK, Rice HE: **Characterization of neuronal/glial differentiation of murine adipose-derived adult stromal cells.** *Exp Neurol* 2004, **187**:319–328.
9. Leu S, Lin YC, Yuen CM, Yen CH, Kao YH, Sun CK, Yip HK: **Adipose-derived mesenchymal stem cells markedly attenuate brain infarct size and improve neurological function in rats.** *J Transl Med* 2010, **8**:63.
10. Ikegame Y, Yamashita K, Hayashi S, Mizuno H, Tawada M, You F, Yamada K, Tanaka Y, Egashira Y, Nakashima S, Yoshimura S, Iwama T: **Comparison of mesenchymal stem cells from adipose tissue and bone marrow for ischemic stroke therapy.** *Cytotherapy* 2011, **13**:675–685.
11. Tan B, Luan Z, Wei X, He Y, Wei G, Johnstone BH, Farlow M, Du Y: **AMP-activated kinase mediates adipose stem cell-stimulated neuritogenesis of PC12 cells.** *Neuroscience* 2011, **181**:40–47.
12. Reid AJ, Sun M, Wiberg M, Downes S: *Terenghi G*. Kingham PJ: Nerve repair with adipose-derived stem cells protects dorsal root ganglia neurons from apoptosis. Neuroscience; 2011.

13. Rehman J, Traktuev D, Li J, Merfeld-Clauss S, Temm-Grove CJ, Bovenkerk JE, Pell CL, Johnstone BH, Considine RV, March KL: **Secretion of angiogenic and antiapoptotic factors by human adipose stromal cells.** *Circulation* 2004, **109**:1292–1298.
14. Lee EY, Xia Y, Kim WS, Kim MH, Kim TH, Kim KJ, Park BS, Sung JH: **Hypoxia-enhanced wound-healing function of adipose-derived stem cells: increase in stem cell proliferation and up-regulation of VEGF and bFGF.** *Wound Repair Regen* 2009, **17**:540–547.
15. Lu S, Lu C, Han Q, Li J, Du Z, Liao L, Zhao RC: **Adipose-derived mesenchymal stem cells protect PC12 cells from glutamate excitotoxicity-induced apoptosis by upregulation of XIAP through PI3-K/Akt activation.** *Toxicology* 2011, **279**:189–195.
16. McCoy MK, Martinez TN, Ruhn KA, Wrage PC, Keefer EW, Botterman BR, Tansey KE, Tansey MG: **Autologous transplants of Adipose-Derived Adult Stromal (ADAS) cells afford dopaminergic neuroprotection in a model of Parkinson's disease.** *Exp Neurol* 2008, **210**:14–29.
17. Flamm ES, Demopoulos HB, Seligman ML, Poser RG, Ransohoff J: **Free radicals in cerebral ischemia.** *Stroke* 1978, **9**:445–447.
18. Alexandrova ML, Bochev PG: **Oxidative stress during the chronic phase after stroke.** *Free Radic Biol Med* 2005, **39**:297–316.
19. Lambeth JD: **NOX enzymes and the biology of reactive oxygen.** *Nat Rev Immunol* 2004, **4**:181–189.
20. Simpson JE, Ince PG, Haynes LJ, Theaker R, Gelsthorpe C, Baxter L, Forster G, Lace GL, Shaw PJ, Matthews FE, Savva GM, Brayne C, Wharton SB, MRC Cognitive Function and Ageing Neuropathology Study Group: **Population variation in oxidative stress and astrocyte DNA damage in relation to Alzheimer-type pathology in the ageing brain.** *Neuropathol Appl Neurobiol* 2010, **36**:25–40.
21. Cai Z, Zhao B, Ratka A: **Oxidative Stress and beta-Amyloid Protein in Alzheimer's Disease.** *Neuromolecular Med* 2011, **13**:223–250.
22. Beal MF: **Mitochondria, oxidative damage, and inflammation in Parkinson's disease.** *Ann N Y Acad Sci* 2003, **991**:120–131.
23. Henchcliffe C, Beal MF: **Mitochondrial biology and oxidative stress in Parkinson disease pathogenesis.** *Nat Clin Pract Neurol* 2008, **4**:600–609.
24. Minghetti L, Ajmone-Cat MA, De Berardinis MA, De Simone R: **Microglial activation in chronic neurodegenerative diseases: roles of apoptotic neurons and chronic stimulation.** *Brain Res Brain Res Rev* 2005, **48**:251–256.
25. Colton CA, Chernyshev ON, Gilbert DL, Vitek MP: **Microglial contribution to oxidative stress in Alzheimer's disease.** *Ann N Y Acad Sci* 2000, **899**:292–307.
26. Hayashi H, Ishisaki A, Suzuki M, Imamura T: **BMP-2 augments FGF-induced differentiation of PC12 cells through upregulation of FGF receptor-1 expression.** *J Cell Sci* 2001, **114**:1387–1395.
27. Hayashi H, Ishisaki A, Imamura T: **Smad mediates BMP-2-induced upregulation of FGF-evoked PC12 cell differentiation.** *FEBS Lett* 2003, **536**:30–34.
28. Son Y, Cheong YK, Kim NH, Chung HT, Kang DG, Pae HO: **Mitogen-Activated Protein Kinases and Reactive Oxygen Species: How Can ROS Activate MAPK Pathways?** *J Signal Transduct* 2011, **2011**:792639.
29. Ito K, Hirao A, Arai F, Takubo K, Matsuoka S, Miyamoto K, Ohmura M, Naka K, Hosokawa K, Ikeda Y, Suda T: **Reactive oxygen species act through p38 MAPK to limit the lifespan of hematopoietic stem cells.** *Nat Med* 2006, **12**:446–451.
30. Raingeaud J, Whitmarsh AJ, Barrett T, Derijard B, Davis RJ: **MKK3- and MKK6-regulated gene expression is mediated by the p38 mitogen-activated protein kinase signal transduction pathway.** *Mol Cell Biol* 1996, **16**:1247–1255.
31. Feng JQ, Xing L, Zhang JH, Zhao M, Horn D, Chan J, Boyce BF, Harris SE, Mundy GR, Chen D: **NF-kappaB specifically activates BMP-2 gene expression in growth plate chondrocytes in vivo and in a chondrocyte cell line in vitro.** *J Biol Chem* 2003, **278**:29130–29135.
32. Vermeulen L, De Wilde G, Van Damme P: **Vanden Berghe W, Haegeman G: Transcriptional activation of the NF-kappaB p65 subunit by mitogen- and stress-activated protein kinase-1 (MSK1).** *EMBO J* 2003, **22**:1313–1324.
33. Rasmussen JG, Frobert O, Pilgaard L, Kastrup J, Simonsen U, Zachar V, Fink T: **Prolonged hypoxic culture and trypsinization increase the pro-angiogenic potential of human adipose tissue-derived stem cells.** *Cytotherapy* 2011, **13**:318–328.
34. Parikh P, Hao Y, Hosseinkhani M, Patil SB, Huntley GW, Tessier-Lavigne M, Zou H: **Regeneration of axons in injured spinal cord by activation of bone morphogenetic protein/Smad1 signaling pathway in adult neurons.** *Proc Natl Acad Sci U S A* 2011, **108**:E99–E107.
35. Ma CH, Brenner GJ, Omura T, Samad OA, Costigan M, Inquimbert P, Niederkofler V, Salie R, Sun CC, Lin HY, Arber S, Coppola G, Woolf CJ, Samad TA: **The BMP coreceptor RGMb promotes while the endogenous BMP antagonist noggin reduces neurite outgrowth and peripheral nerve regeneration by modulating BMP signaling.** *J Neurosci* 2011, **31**:18391–18400.
36. Jordan J, Bottner M, Schluesener HJ, Unsicker K, Krieglstein K: **Bone morphogenetic proteins: neurotrophic roles for midbrain dopaminergic neurons and implications of astroglial cells.** *Eur J Neurosci* 1997, **9**:1699–1709.
37. Reiriz J, Espejo M, Ventura F, Ambrosio S, Alberch J: **Bone morphogenetic protein-2 promotes dissociated effects on the number and differentiation of cultured ventral mesencephalic dopaminergic neurons.** *J Neurobiol* 1999, **38**:161–170.
38. Stull ND, Jung JW, Iacovitti L: **Induction of a dopaminergic phenotype in cultured striatal neurons by bone morphogenetic proteins.** *Brain Res Dev Brain Res* 2001, **130**:91–98.
39. Anitha M, Shahnavaz N, Qayed E, Joseph I, Gossrau G, Mwangi S, Sitaraman SV, Greene JG, Srinivasan S: **BMP2 promotes differentiation of nitrergic and catecholaminergic enteric neurons through a Smad1-dependent pathway.** *Am J Physiol Gastrointest Liver Physiol* 2010, **298**:G375–G383.
40. Ikeda N, Nonoguchi N, Zhao MZ, Watanabe T, Kajimoto Y, Furutama D, Kimura F, Dezawa M, Coffin RS, Otsuki Y, Kuroiwa T, Miyatake S: **Bone marrow stromal cells that enhanced fibroblast growth factor-2 secretion by herpes simplex virus vector improve neurological outcome after transient focal cerebral ischemia in rats.** *Stroke* 2005, **36**:2725–2730.
41. Viemann D, Goebeler M, Schmid S, Klimmek K, Sorg C, Ludwig S, Roth J: **Transcriptional profiling of IKK2/NF-kappa B- and p38 MAP kinase-dependent gene expression in TNF-alpha-stimulated primary human endothelial cells.** *Blood* 2004, **103**:3365–3373.
42. Hotokezaka H, Sakai E, Kanaoka K, Saito K, Matsuo K, Kitaura H, Yoshida N, Nakayama K: **U0126 and PD98059, specific inhibitors of MEK, accelerate differentiation of RAW264.7 cells into osteoclast-like cells.** *J Biol Chem* 2002, **277**:47366–47372.
43. Shimo T, Matsumura S, Ibaragi S, Isowa S, Kishimoto K, Mese H, Nishiyama A, Sasaki A: **Specific inhibitor of MEK-mediated cross-talk between ERK and p38 MAPK during differentiation of human osteosarcoma cells.** *J Cell Commun Signal* 2007, **1**:103–111.
44. Al-Shanti N, Stewart CE: **PD98059 enhances C2 myoblast differentiation through p38 MAPK activation: a novel role for PD98059.** *J Endocrinol* 2008, **198**:243–252.
45. Okura H, Saga A, Fumimoto Y, Soeda M, Moriyama M, Moriyama H, Nagai K, Lee CM, Yamashita S, Ichinose A, Hayakawa T, Matsuyama A: **Transplantation of human adipose tissue-derived multilineage progenitor cells reduces serum cholesterol in hyperlipidemic Watanabe rabbits.** *Tissue Eng Part C Methods* 2011, **17**:145–154.
46. Saga A, Okura H, Soeda M, Tani J, Fumimoto Y, Komoda H, Moriyama M, Moriyama H, Yamashita S, Ichinose A, Daimon T, Hayakawa T, Matsuyama A: **HMG-CoA reductase inhibitor augments the serum total cholesterol-lowering effect of human adipose tissue-derived multilineage progenitor cells in hyperlipidemic homozygous Watanabe rabbits.** *Biochem Biophys Res Commun* 2011, **412**:50–54.

doi:10.1186/1471-2121-13-21
Cite this article as: Moriyama *et al.*: Human adipose tissue-derived multilineage progenitor cells exposed to oxidative stress induce neurite outgrowth in PC12 cells through p38 MAPK signaling. *BMC Cell Biology* 2012 13:21.

EASL EUROPEAN ASSOCIATION FOR THE STUDY OF THE LIVER | JOURNAL OF HEPATOLOGY

Generation of metabolically functioning hepatocytes from human pluripotent stem cells by FOXA2 and HNF1α transduction

Kazuo Takayama[1,2], Mitsuru Inamura[1,2], Kenji Kawabata[2,3], Michiko Sugawara[4], Kiyomi Kikuchi[4], Maiko Higuchi[2], Yasuhito Nagamoto[1,2], Hitoshi Watanabe[1,2], Katsuhisa Tashiro[2], Fuminori Sakurai[1], Takao Hayakawa[5,6], Miho Kusuda Furue[7,8], Hiroyuki Mizuguchi[1,2,9,*]

[1]*Laboratory of Biochemistry and Molecular Biology, Graduate School of Pharmaceutical Sciences, Osaka University, Osaka 565-0871, Japan;* [2]*Laboratory of Stem Cell Regulation, National Institute of Biomedical Innovation, Osaka 567-0085, Japan;* [3]*Laboratory of Biomedical Innovation, Graduate School of Pharmaceutical Sciences, Osaka University, Osaka 565-0871, Japan;* [4]*Tsukuba Laboratories, Eisai Co., Ltd., Ibaraki 300-2635, Japan;* [5]*Pharmaceutics and Medical Devices Agency, Tokyo 100-0013, Japan;* [6]*Pharmaceutical Research and Technology Institute, Kinki University, Osaka 577-8502, Japan;* [7]*Laboratory of Cell Cultures, Department of Disease Bioresources Research, National Institute of Biomedical Innovation, Osaka 567-0085, Japan;* [8]*Laboratory of Cell Processing, Institute for Frontier Medical Sciences, Kyoto University, Kyoto 606-8507, Japan;* [9]*The Center for Advanced Medical Engineering and Informatics, Osaka University, Osaka 565-0871, Japan*

Background & Aims: Hepatocyte-like cells differentiated from human embryonic stem cells (hESCs) and induced pluripotent stem cells (hiPSCs) can be utilized as a tool for screening for hepatotoxicity in the early phase of pharmaceutical development. We have recently reported that hepatic differentiation is promoted by sequential transduction of SOX17, HEX, and HNF4α into hESC- or hiPSC-derived cells, but further maturation of hepatocyte-like cells is required for widespread use of drug screening.
Methods: To screen for hepatic differentiation-promoting factors, we tested the seven candidate genes related to liver development.
Results: The combination of two transcription factors, FOXA2 and HNF1α, promoted efficient hepatic differentiation from hESCs and hiPSCs. The expression profile of hepatocyte-related genes (such as genes encoding cytochrome P450 enzymes, conjugating enzymes, hepatic transporters, and hepatic nuclear receptors) achieved with FOXA2 and HNF1α transduction was comparable to that obtained in primary human hepatocytes. The hepatocyte-like cells generated by FOXA2 and HNF1α transduction exerted various hepatocyte functions including albumin and urea secretion, and the uptake of indocyanine green and low density lipoprotein. Moreover, these cells had the capacity to metabolize all nine tested drugs and were successfully employed to evaluate drug-induced cytotoxicity.
Conclusions: Our method employing the transduction of FOXA2 and HNF1α represents a useful tool for the efficient generation of metabolically functional hepatocytes from hESCs and hiPSCs, and the screening of drug-induced cytotoxicity.

© 2012 European Association for the Study of the Liver. Published by Elsevier B.V. All rights reserved.

Keywords: FOXA2; HNF1α; Hepatocytes; Adenovirus; Drug screening; Drug metabolism; hESCs; hiPSCs.
Received 14 November 2011; received in revised form 31 March 2012; accepted 4 April 2012; available online 29 May 2012
* Corresponding author. Address: Laboratory of Biochemistry and Molecular Biology, Graduate School of Pharmaceutical Sciences, Osaka University, 1-6 Yamadaoka, Suita, Osaka 565-0871, Japan. Tel.: +81 6 6879 8185; fax: +81 6 6879 8186.
E-mail address: mizuguch@phs.osaka-u.ac.jp (H. Mizuguchi).

Introduction

Hepatocyte-like cells differentiated from human embryonic stem cells (hESCs) [1] or human induced pluripotent stem cells (hiPSCs) [2] have more advantages than primary human hepatocytes (PHs) for drug screening. While application of PHs in drug screening has been hindered by lack of cellular growth, loss of function, and de-differentiation *in vitro* [3], hESC- or hiPSC-derived hepatocyte-like cells (hESC-hepa or hiPSC-hepa, respectively) have potential to solve these problems.

Hepatic differentiation from hESCs and hiPSCs can be divided into four stages: definitive endoderm (DE) differentiation, hepatic commitment, hepatic expansion, and hepatic maturation. Various growth factors are required to mimic liver development [4] and to promote hepatic differentiation. Previously, we showed that transduction of transcription factors in addition to treatment with optimal growth factors was effective to enhance hepatic differentiation [5–7]. An almost homogeneous hepatocyte population was obtained by sequential transduction of SOX17, HEX, and HNF4α into hESC- or hiPSCs-derived cells [7]. However, further maturation of the hESC-hepa and hiPSC-hepa is required for widespread use of drug screening because the drug metabolism capacity of these cells was not sufficient.

In some previous reports, hESC-hepa and hiPSC-hepa have been characterized for their hepatocyte functions in numerous ways, including functional assessment such as glycogen storage and low density lipoprotein (LDL) uptake [7]. To make a more precise judgment as to whether hESC-hepa and hiPSC-hepa can be applied to drug screening, it is more important to assess cytochrome P450 (CYP) induction potency and drug metabolism capacity rather than general hepatocyte function. Although Duan *et al.* have examined the drug metabolism capacity of hESC-hepa, drug metabolites were measured at 24 or 48 h [8]. To precisely

ELSEVIER

13. Rehman J, Traktuev D, Li J, Merfeld-Clauss S, Temm-Grove CJ, Bovenkerk JE, Pell CL, Johnstone BH, Considine RV, March KL: Secretion of angiogenic and antiapoptotic factors by human adipose stromal cells. *Circulation* 2004, 109:1292–1298.
14. Lee EY, Xia Y, Kim WS, Kim MH, Kim TH, Kim KJ, Park BS, Sung JH: Hypoxia-enhanced wound-healing function of adipose-derived stem cells: increase in stem cell proliferation and up-regulation of VEGF and bFGF. *Wound Repair Regen* 2009, 17:540–547.
15. Lu S, Lu C, Han Q, Li J, Du Z, Liao L, Zhao RC: Adipose-derived mesenchymal stem cells protect PC12 cells from glutamate excitotoxicity-induced apoptosis by upregulation of XIAP through PI3-K/Akt activation. *Toxicology* 2011, 279:189–195.
16. McCoy MK, Martinez TN, Ruhn KA, Wrage PC, Keefer EW, Botterman BR, Tansey KE, Tansey MG: Autologous transplants of Adipose-Derived Adult Stromal (ADAS) cells afford dopaminergic neuroprotection in a model of Parkinson's disease. *Exp Neurol* 2008, 210:14–29.
17. Flamm ES, Demopoulos HB, Seligman ML, Poser RG, Ransohoff J: Free radicals in cerebral ischemia. *Stroke* 1978, 9:445–447.
18. Alexandrova ML, Bochev PG: Oxidative stress during the chronic phase after stroke. *Free Radic Biol Med* 2005, 39:297–316.
19. Lambeth JD: NOX enzymes and the biology of reactive oxygen. *Nat Rev Immunol* 2004, 4:181–189.
20. Simpson JE, Ince PG, Haynes LJ, Theaker R, Gelsthorpe C, Baxter L, Forster G, Lace GL, Shaw PJ, Matthews FE, Savva GM, Brayne C, Wharton SB, MRC Cognitive Function and Ageing Neuropathology Study Group: Population variation in oxidative stress and astrocyte DNA damage in relation to Alzheimer-type pathology in the ageing brain. *Neuropathol Appl Neurobiol* 2010, 36:25–40.
21. Cai Z, Zhao B, Ratka A: Oxidative Stress and beta-Amyloid Protein in Alzheimer's Disease. *Neuromolecular Med* 2011, 13:223–250.
22. Beal MF: Mitochondria, oxidative damage, and inflammation in Parkinson's disease. *Ann N Y Acad Sci* 2003, 991:120–131.
23. Henchcliffe C, Beal MF: Mitochondrial biology and oxidative stress in Parkinson disease pathogenesis. *Nat Clin Pract Neurol* 2008, 4:600–609.
24. Minghetti L, Ajmone-Cat MA, De Berardinis MA, De Simone R: Microglial activation in chronic neurodegenerative diseases: roles of apoptotic neurons and chronic stimulation. *Brain Res Brain Res Rev* 2005, 48:251–256.
25. Colton CA, Chernyshev ON, Gilbert DL, Vitek MP: Microglial contribution to oxidative stress in Alzheimer's disease. *Ann N Y Acad Sci* 2000, 899:292–307.
26. Hayashi H, Ishisaki A, Suzuki M, Imamura T: BMP-2 augments FGF-induced differentiation of PC12 cells through upregulation of FGF receptor-1 expression. *J Cell Sci* 2001, 114:1387–1395.
27. Hayashi H, Ishisaki A, Imamura T: Smad mediates BMP-2-induced upregulation of FGF-evoked PC12 cell differentiation. *FEBS Lett* 2003, 536:30–34.
28. Son Y, Cheong YK, Kim NH, Chung HT, Kang DG, Pae HO: Mitogen-Activated Protein Kinases and Reactive Oxygen Species: How Can ROS Activate MAPK Pathways? *J Signal Transduct* 2011, 2011:792639.
29. Ito K, Hirao A, Arai F, Takubo K, Matsuoka S, Miyamoto K, Ohmura M, Naka K, Hosokawa K, Ikeda Y, Suda T: Reactive oxygen species act through p38 MAPK to limit the lifespan of hematopoietic stem cells. *Nat Med* 2006, 12:446–451.
30. Raingeaud J, Whitmarsh AJ, Barrett T, Derijard B, Davis RJ: MKK3- and MKK6-regulated gene expression is mediated by the p38 mitogen-activated protein kinase signal transduction pathway. *Mol Cell Biol* 1996, 16:1247–1255.
31. Feng JQ, Xing L, Zhang JH, Zhao M, Horn D, Chan J, Boyce BF, Harris SE, Mundy GR, Chen D: NF-kappaB specifically activates BMP-2 gene expression in growth plate chondrocytes in vivo and in a chondrocyte cell line in vitro. *J Biol Chem* 2003, 278:29130–29135.
32. Vermeulen L, De Wilde G, Van Damme P: Vanden Berghe W, Haegeman G: Transcriptional activation of the NF-kappaB p65 subunit by mitogen- and stress-activated protein kinase-1 (MSK1). *EMBO J* 2003, 22:1313–1324.
33. Rasmussen JG, Frobert O, Pilgaard L, Kastrup J, Simonsen U, Zachar V, Fink T: Prolonged hypoxic culture and trypsinization increase the pro-angiogenic potential of human adipose tissue-derived stem cells. *Cytotherapy* 2011, 13:318–328.
34. Parikh P, Hao Y, Hosseinkhani M, Patil SB, Huntley GW, Tessier-Lavigne M, Zou H: Regeneration of axons in injured spinal cord by activation of bone morphogenetic protein/Smad1 signaling pathway in adult neurons. *Proc Natl Acad Sci U S A* 2011, 108:E99–E107.
35. Ma CH, Brenner GJ, Omura T, Samad OA, Costigan M, Inquimbert P, Niederkofler V, Salie R, Sun CC, Lin HY, Arber S, Coppola G, Woolf CJ, Samad TA: The BMP coreceptor RGMb promotes while the endogenous BMP antagonist noggin reduces neurite outgrowth and peripheral nerve regeneration by modulating BMP signaling. *J Neurosci* 2011, 31:18391–18400.
36. Jordan J, Bottner M, Schluesener HJ, Unsicker K, Krieglstein K: Bone morphogenetic proteins: neurotrophic roles for midbrain dopaminergic neurons and implications of astroglial cells. *Eur J Neurosci* 1997, 9:1699–1709.
37. Reiriz J, Espejo M, Ventura F, Ambrosio S, Alberch J: Bone morphogenetic protein-2 promotes dissociated effects on the number and differentiation of cultured ventral mesencephalic dopaminergic neurons. *J Neurobiol* 1999, 38:161–170.
38. Stull ND, Jung JW, Iacovitti L: Induction of a dopaminergic phenotype in cultured striatal neurons by bone morphogenetic proteins. *Brain Res Dev Brain Res* 2001, 130:91–98.
39. Anitha M, Shahnavaz N, Qayed E, Joseph I, Gossrau G, Mwangi S, Sitaraman SV, Greene JG, Srinivasan S: BMP2 promotes differentiation of nitrergic and catecholaminergic enteric neurons through a Smad1-dependent pathway. *Am J Physiol Gastrointest Liver Physiol* 2010, 298:G375–G383.
40. Ikeda N, Nonoguchi N, Zhao MZ, Watanabe T, Kajimoto Y, Furutama D, Kimura F, Dezawa M, Coffin RS, Otsuki Y, Kuroiwa T, Miyatake S: Bone marrow stromal cells that enhanced fibroblast growth factor-2 secretion by herpes simplex virus vector improve neurological outcome after transient focal cerebral ischemia in rats. *Stroke* 2005, 36:2725–2730.
41. Viemann D, Goebeler M, Schmid S, Klimmek K, Sorg C, Ludwig S, Roth J: Transcriptional profiling of IKK2/NF-kappa B- and p38 MAP kinase-dependent gene expression in TNF-alpha-stimulated primary human endothelial cells. *Blood* 2004, 103:3365–3373.
42. Hotokezaka H, Sakai E, Kanaoka K, Saito K, Matsuo K, Kitaura H, Yoshida N, Nakayama K: U0126 and PD98059, specific inhibitors of MEK, accelerate differentiation of RAW264.7 cells into osteoclast-like cells. *J Biol Chem* 2002, 277:47366–47372.
43. Shimo T, Matsumura S, Ibaragi S, Isowa S, Kishimoto K, Mese H, Nishiyama A, Sasaki A: Specific inhibitor of MEK-mediated cross-talk between ERK and p38 MAPK during differentiation of human osteosarcoma cells. *J Cell Commun Signal* 2007, 1:103–111.
44. Al-Shanti N, Stewart CE: PD98059 enhances C2 myoblast differentiation through p38 MAPK activation: a novel role for PD98059. *J Endocrinol* 2008, 198:243–252.
45. Okura H, Saga A, Fumimoto Y, Soeda M, Moriyama M, Moriyama H, Nagai K, Lee CM, Yamashita S, Ichinose A, Hayakawa T, Matsuyama A: Transplantation of human adipose tissue-derived multilineage progenitor cells reduces serum cholesterol in hyperlipidemic Watanabe rabbits. *Tissue Eng Part C Methods* 2011, 17:145–154.
46. Saga A, Okura H, Soeda M, Tani J, Fumimoto Y, Komoda H, Moriyama M, Moriyama H, Yamashita S, Ichinose A, Daimon T, Hayakawa T, Matsuyama A: HMG-CoA reductase inhibitor augments the serum total cholesterol-lowering effect of human adipose tissue-derived multilineage progenitor cells in hyperlipidemic homozygous Watanabe rabbits. *Biochem Biophys Res Commun* 2011, 412:50–54.

doi:10.1186/1471-2121-13-21
Cite this article as: Moriyama *et al.*: Human adipose tissue-derived multilineage progenitor cells exposed to oxidative stress induce neurite outgrowth in PC12 cells through p38 MAPK signaling. *BMC Cell Biology* 2012 13:21.